ACS OMEGA

Open Access

http://pubs.acs.org/journal/acsodf

Article

Natural Prenylflavones from the Stem Bark of *Artocarpus altilis*: Promising Anticancer Agents for Oral Squamous Cell Carcinoma Targeting the Akt/mTOR/STAT-3 Signaling Pathway

Maniyamma Aswathy,[⊥] Dey Parama,[⊥] Mangala Hegde, Sherin DR, Ravi S. Lankalapalli, Kokkuvayil Vasu Radhakrishnan,* and Ajaikumar B. Kunnumakkara*

Cite This: *ACS Omega* 2024, 9, 24252−24267

Read Online

ACCESS | Metrics & More | Article Recommendations | Supporting Information

ABSTRACT: Artonin E (AA2) and artobiloxanthone (AA3) were extracted and purified from the acetone extract of the stem bark of *Artocarpus altilis* (Parkinson) Fosberg. Preliminary investigations of both candidates revealed promising cytotoxic effects in oral cancer cells. Moreover, these candidates modulated the expression of pivotal proteins linked to oral cancer progression, eliciting apoptosis through caspase-3 and caspase-9 activation. Additionally, our results showed that AA2 and AA3 suppressed several proteins linked with oral cancer, such as Bcl-2, COX-2, VEGF, and MMP-9, and modulated the cell signaling pathways, such as Akt/mTOR and STAT-3, offering valuable insights into the underlying mechanism of action of these compounds. These findings were robustly validated *in silico* using molecular docking and molecular dynamic simulations. To our knowledge, these findings have not been previously reported, and the continued exploration and development of these natural products may offer a potential avenue for the effective management of this malignancy.

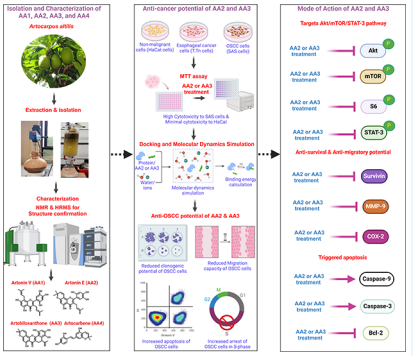

1. INTRODUCTION

Oral squamous cell carcinoma (OSCC) or oral cancer is characterized by squamous cell differentiation resulting from various genetic mutations.[1] OSCC represents a globally prevalent malignancy within head and neck squamous cell carcinoma (HNSCC), which is associated with high morbidity and mortality.[2] According to GLOBOCAN 2020, there were nearly 377,713 new incidences and 177,757 mortalities of oral cancer globally in 2020.[3] Primary etiological factors contributing to the progression of OSCC include consumption of alcohol, betel quid and areca nut, tobacco smoking, viral infection, high intake of unhealthy foods, etc.[4−7] The conventional methods of treatment for oral cancer, encompassing surgery, radiotherapy, chemotherapy, and targeted therapy, have notable limitations, including harmful side effects, tumor recurrence, chemoresistance, and radioresistance.[8,9] Hence, there is an urgent requirement to develop better treatment approaches that can hinder specific pathways individually or in combination, which is crucial for impeding the development and progression of OSCC without causing adverse side effects. The exploration of natural secondary metabolites has significant potential for developing new chemotherapeutic agents for the prevention and treatment of oral cancer.[10−12] In the pursuit of uncovering the substantial biological potential inherent in these functional moieties, we embarked on an exploration of the natural world, commencing our endeavor by isolating phytochemicals from traditionally emphasized floras, with the aim of addressing and alleviating a spectrum of infectious and lifestyle diseases.[13−16]

Phytochemicals are known for their diverse chemical compositions, intricate structures, and pleiotropy, which have rendered them promising candidates for pharmacotherapy since ancient times.[17−19] Many of the isolated phytochemical entities sourced from diverse ethnomedicinal plants possess potential anticancer activities with enhanced selectivity toward cancer cells.[20−23] Consequently, it led to the development of novel chemotherapeutic drugs with broad implications for mankind.[24−26] The widespread accessibility of various plant species, straightforward extraction, isolation and purification methods, nontoxic nature, and the inherent manifestation of multiple pharmacological activities in these species collectively contribute to the establishment of environmentally sustainable and economical drug discovery processes.[27] Our previous report had highlighted the efficacy of the bioactive triterpenoids, namely, betulinic acid and koetjapic acid, extracted from *Dillenia indica* in suppressing the survival and proliferation of oral cancer cells, bridging traditional insight with scientific authentication.[28]

The *Artocarpus* genus comprises around 50 species of both evergreen and deciduous trees, finding diverse applications in

Received: October 24, 2023
Revised: April 19, 2024
Accepted: April 29, 2024
Published: May 24, 2024

Scheme 1. Flavones from AA Displayed Potential Anticancer Activity by Inducing Cell-Cycle Arrest and Apoptosis and Inhibiting the Invasion and Migration of Oral Cancer Cells through Modulating the Expressions of Bcl-2, Caspases, COX-2, and MMP-9 and Suppressing the Activation of Akt/mTOR and STAT-3 Signaling Pathways. This Figure Was Created with BioRender.com

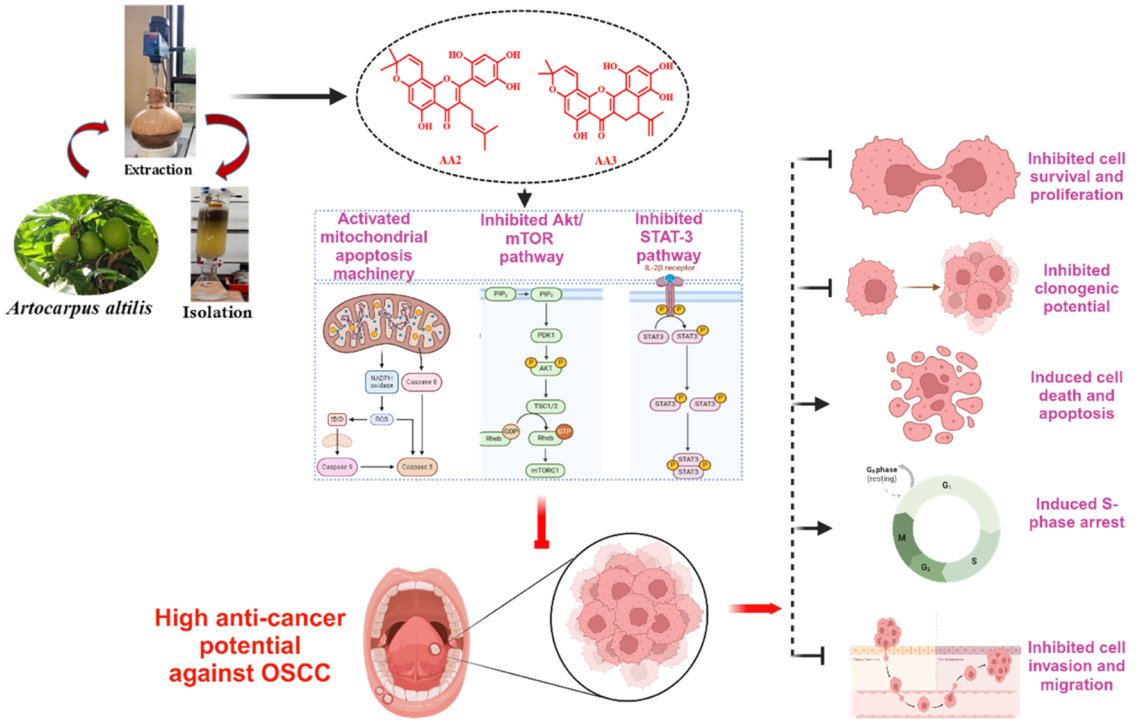

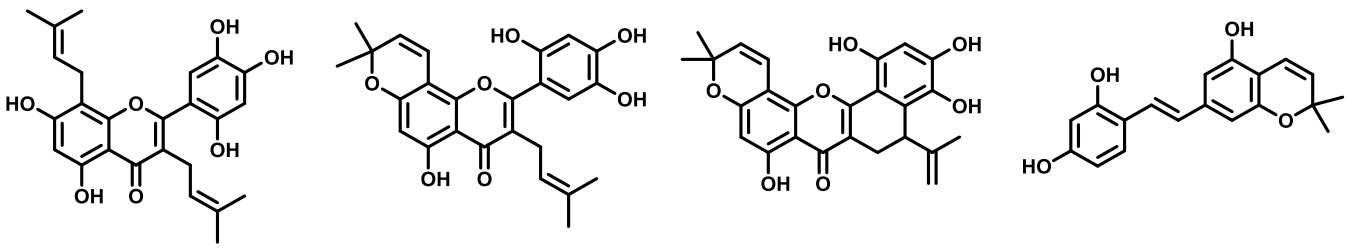

Figure 1. Structure of isolated molecules from the acetone extract of AA stem bark.

various domains, including staple crop cultivation, construction material sourcing, animal feed production, and utilization in traditional medicinal practices.[29] Furthermore, specific species within this genus, such as *Artocarpus heterophyllus*, *Artocarpus camansi*, *Artocarpus hirsutus*, and *Artocarpus altilis*, are renowned for their edible aggregate fruits. Traditionally, *A. altilis* (Parkinson) Fosberg. (AA) holds significance in agroforestry systems indigenous to tropical and Pacific Asia, with cultivation extending across humid tropical regions. The leaves of AA are commonly employed in traditional medicine for conditions like hypertension, liver cirrhosis, and diabetes.[29] Apart from its culinary attributes, AA contains a wide variety of phytochemicals, mainly aromatic compounds like flavonoids, stilbenoids, and arylbenzofurans.[30,31] Isoprenyl and geranyl flavones from AA have shown diverse biological effects including antibacterial, antihelminthic, antihypertensive, antioxidant, antiplasmodial, and antitubercular activities.[32] These findings highlight the potential pharmacological significance of this plant species in various therapeutic applications.

Artonin E, also known as 5′-hydroxymorusin, possesses a flavonoid skeleton linked to a lipophilic prenyl side chain. Initially detected in the bark of AA, this molecule has been widely explored for its varied pharmacological activities, encompassing antibacterial,[33] anticancer,[34] antiestrogenic,[35] anti-FAT10,[36] antimalarial,[37] antinephritis,[35] antioxidant,[35] and antiplasmodial activities.[38] The anticancer effects of Artonin E have been explored across diverse cancer cell types, including breast (MCF-7, MDA-MB-231),[39,40] colon (LoVo, HCT116),[41,42] gastric cancers (AGS),[43] leukemia (P-388),[44] lung (H460, H23, H292, A549),[45,46] and ovarian (SKOV3, 1A9).[47,48] These studies highlight the potential of artonin E in inducing apoptosis, anoikis, and cell-cycle arrest and inhibiting proliferation, invasion, migration, and overcoming resistance to the tumor necrosis factor-related apoptosis-inducing ligand (TRAIL).[39−49] The underlying mechanisms involve activation and suppression of proapoptotic and antiapoptotic proteins, respectively.

Artobiloxanthone, an organic aromatic compound of the pyranoxanthone class, is distinguished by its fused pyranoxanthone ring system.[50] Comprehensive investigations, as documented on SpringerLink, shed light on its noteworthy affinity for transglutaminase 2 (TG2), a protein implicated in

https://doi.org/10.1021/acsomega.3c08376
ACS Omega 2024, 9, 24252−24267

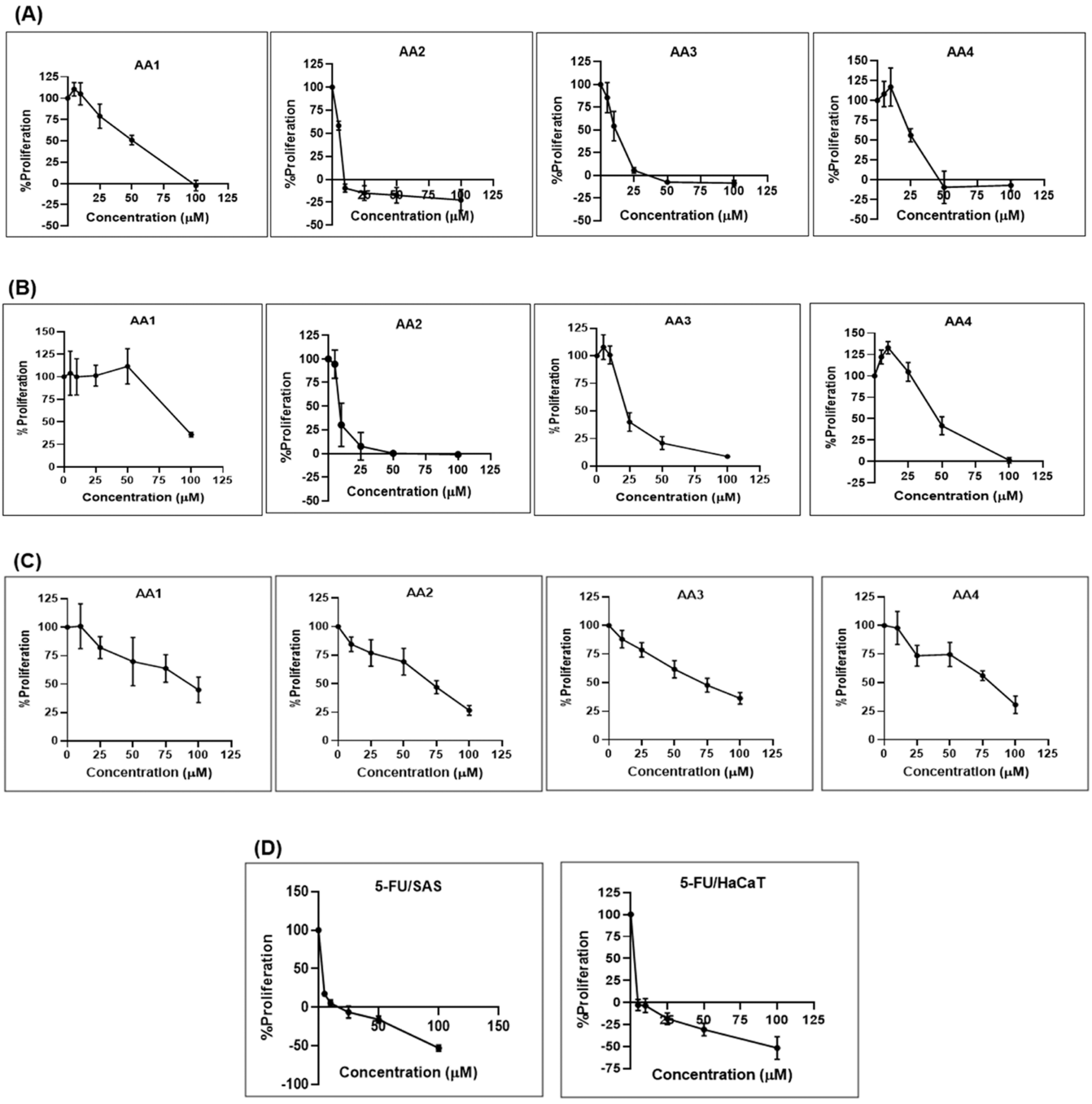

Figure 2. Antiproliferative potential of the compounds isolated from AA on cancer cells. The antiproliferative activity of the compounds AA1−4 was examined using MTT assay in different cell lines for 72 h: (A) SAS (0, 5, 10, 25, 50, 100 μM), (B) T.Tn (0, 5, 10, 25, 50, 100 μM), and (C) HaCaT cells (0, 10, 25, 50, 75, 100 μM). (D) 5-FU was used as a positive control (0, 5, 10, 25, 50, 100 μM). %proliferation of the control was taken as 100%, and the graphs were plotted using GraphPad Prism 9.0.

various diseases, including lung cancer.[51] This compound demonstrates inhibitory effects on cell growth, kinase activity, apoptosis induction, and the suppression of tumor invasion.[29,31,51,52] In the present study, we have isolated four compounds from AA and examined their effects in regulating the various hallmarks of oral cancer and the mechanism responsible for their anticancer effect. To our current understanding, this study marks the primary evaluation of the anticancer potential of these compounds isolated from AA in OSCC (Scheme 1).

2. RESULTS AND DISCUSSION

2.1. Isolation of AA1, AA2, AA3, and AA4 from the Stem Bark of AA. The acetone extract of AA (900 g) was obtained through percolation from a defatted stem bark. Subsequently, the crude extract underwent fractionation, and purification was done with silica gel column chromatography with different gradients of hexane and ethyl acetate mixtures. This resulted in the isolation of artonin E (AA2) and artobiloxanthone (AA3) as a yellow-colored solid and brown syrup, respectively (Figure 1). Two other flavonoids, namely, artonin V (AA1) and artocarbene (AA4), were also identified

https://doi.org/10.1021/acsomega.3c08376
ACS Omega 2024, 9, 24252−24267

(Figure 1). The structural elucidation of these compounds was confirmed through spectroscopic techniques, such as ^{1}H NMR, ^{13}C NMR, and ESI-HRMS (Figure S1−S6).

2.2. Evaluation of the Antiproliferative Potential of Isolated Phytochemicals against Human Cancerous and Normal Cell Lines. In the initial phase of our investigation, we determined the antiproliferative efficacy of isolated compounds, namely, AA1, AA2, AA3, and AA4, against the OSCC cell line SAS and the esophageal cancer cell line T.Tn *in vitro* using the 3-[4,5-dimethylthiazol-2-yl]-2,5 diphenyl tetrazolium bromide (MTT) assay. Remarkably, a pronounced decrease in cell proliferation was observed in a concentration-dependent manner after the treatment of SAS and T.Tn cells with these compounds. The IC_{50} values for AA1, AA2, AA3, and AA4 in SAS cells were found to be 50, 6, 11, and 22 μM, respectively (Figure 2A) (Table 1), while in T.Tn cells, the corresponding concentrations were 92, 8, 22, and 46 μM, respectively, following a 72 h incubation period (Figure 2B) (Table 1). We have also analyzed the antiproliferative effect of these compounds on the human normal cell line HaCaT to confirm their selectivity. Surprisingly, we observed that the IC_{50} concentrations of these compounds on HaCaT cells were much higher than those of SAS and T.Tn cells. The IC_{50} values for AA1, AA2, AA3, and AA4 on HaCaT cells were found to be 92, 72, 70, and 80 μM, respectively, suggesting that these compounds are highly selective for SAS and T.Tn cells (Figure 2C) (Table 1). We also evaluated the effect of 5-fluorouracil (5-FU), a common chemotherapeutic agent for OSCC, on SAS and HaCaT cells. The IC_{50} values of 5-FU on SAS and HaCaT cells were found to be 3 and 4 μM, respectively (Figure 2D) (Table 1). Next, we analyzed the selectivity index (SI) for the compounds and 5-FU. SI is defined as a compound's potential to preferentially target cancer cells while minimizing its impact on normal cells, and it is measured as a ratio of the cytotoxic concentration of a compound (IC_{50} value in noncancerous cells) to its effective bioactive concentration (IC_{50} value in cancerous cells).[53] SI values for AA1, AA2, AA3, AA4, and 5-FU were found to be 1.8, 12, 6.4, 3.6, and 1.3, respectively (Table 1). An SI value of 3 or higher was proposed to be indicative of a potential anticancer compound.[54] Therefore, based on our studies, it could be inferred that AA2 and AA3 exhibited higher selectivity than the other compounds toward SAS cells as compared to HaCaT cells and thus qualify to be further screened for being developed as potential anticancer therapeutics.

Table 1. Antiproliferative Potential of Compounds Isolated from AA against Various Cell Lines Represented in Terms of Their IC_{50} and SI Values

	IC_{50} value (μM)			Selectivity index (SI)
Compounds	SAS	T.Tn	HaCaT	IC_{50} (HaCaT)/IC_{50} (SAS)
AA1	50	92	92	1.8
AA2	6	8	72	12
AA3	11	22	70	6.4
AA4	22	46	80	3.6
5-FU	3		4	1.3

From our study, it was also observed that 5-FU displayed a weak SI value of 1.3. Despite being in use for over five decades, a handful of studies have reported the adverse side effects of 5-FU such as drug resistance, peripheral neuropathy, oral mucositis, nausea, vomiting, and hair loss.[55,56] In addition, studies have also reported cognitive impairment as a long-term side-effect associated with 5-FU.[57] Therefore, based on our study, it can be proposed that AA2 and AA3 demonstrated promising effects with enhanced selectivity toward cancer cells and minimal cytotoxicity against noncancerous cells when compared to the standard chemotherapeutic drug 5-FU.

Since the compounds AA2 and AA3 exhibited higher selectivity in comparison to AA1 and AA4, subsequent studies were conducted using these compounds. Moreover, these compounds demonstrated greater efficacy toward SAS cells in contrast to T.Tn cells. Consequently, this paper aimed to assess the impact of AA2 and AA3 specifically on the OSCC cell line SAS.

2.3. Computational Screening of Active Candidates AA2 and AA3. To comprehensively interpret our experimental findings, we conducted computational screening utilizing molecular docking techniques for active candidates AA2 and AA3. This approach aimed to predict the binding affinity of these molecules for specific protein domains known to regulate various hallmarks of cancer. Additionally, molecular dynamics simulations were used to assess the flexibility and compatibility of AA2 and AA3 within the binding pockets of the selected receptors. By integrating computational analysis with experimental data, we aimed to improve our understanding of the molecular interactions behind the potential therapeutic effects of these compounds on cancer regulation. This multifaceted approach strengthens the validity and depth of our research findings, providing valuable insights into the mechanisms of action of AA2 and AA3 as potential anticancer agents.

2.3.1. Molecular Docking. In this study, we utilized molecular docking to evaluate the binding affinities of AA2 and AA3 with key proteins involved in cancer progression. These ligands were docked against a carefully selected set of seven proteins, which are involved in various stages of cancer development, including Akt (PDB ID: 1O6L), B-cell lymphoma 2 (Bcl-2) (PDB ID: 2O21), caspase-3 (PDB ID: 1GFW), caspase-9 (PDB ID: 1JXQ), cyclooxygenase 2 (COX-2) (PDB ID: 1PXX), mammalian target of rapamycin (mTOR) (PDB ID: 4JSP), and p53 (PDB ID: 1TUP). These selections were based on their critical involvement in essential cellular processes linked to cancer such as apoptosis, cell proliferation, and angiogenesis.

Our docking analyses unveiled significant interactions between AA2 and AA3 and several target proteins. Noteworthy was AA2′s strong binding affinity with Bcl-2, caspase-3, and caspase-9, yielding docking scores of −8.2, −8.2, and −7.4 kcal/mol, respectively. In the case of 1GFW, the strong docking score of −8.2 kcal/mol can be attributed to hydrogen-bonding interactions between AA2′s hydroxyl groups and the polar amino acid residue SER209, along with hydrophobic interactions with PHE250. Likewise, the interaction with caspase-9, resulting in a maximum binding energy of −7.4 kcal/mol, is facilitated by a hydrogen-bond (H-bond) interaction between AA2′s hydroxyl group and the amino acid residue PHE294. Additionally, AA2 effectively binds to Bcl-2 through the formation of two H-bonds with GLU133 and ALA146, leading to a maximum binding energy of −8.2 kcal/mol (Figures S6−S8, Supporting Information). Similarly, AA3 demonstrates significant binding affinity, particularly with caspase-3, with a docking score of −7.9 kcal/mol, and with caspase-9 and Bcl-2, with scores of −7.8 and −7.4 kcal/mol, respectively (Figures S6−S8). The enhanced binding affinity of AA3 with these proteins can be attributed to H-bond interactions involving the polar hydroxyl groups of the ligand and various amino acid residues, such as ARG207 and HIS292 (Figures S6−S8).

https://doi.org/10.1021/acsomega.3c08376
ACS Omega 2024, 9, 24252−24267

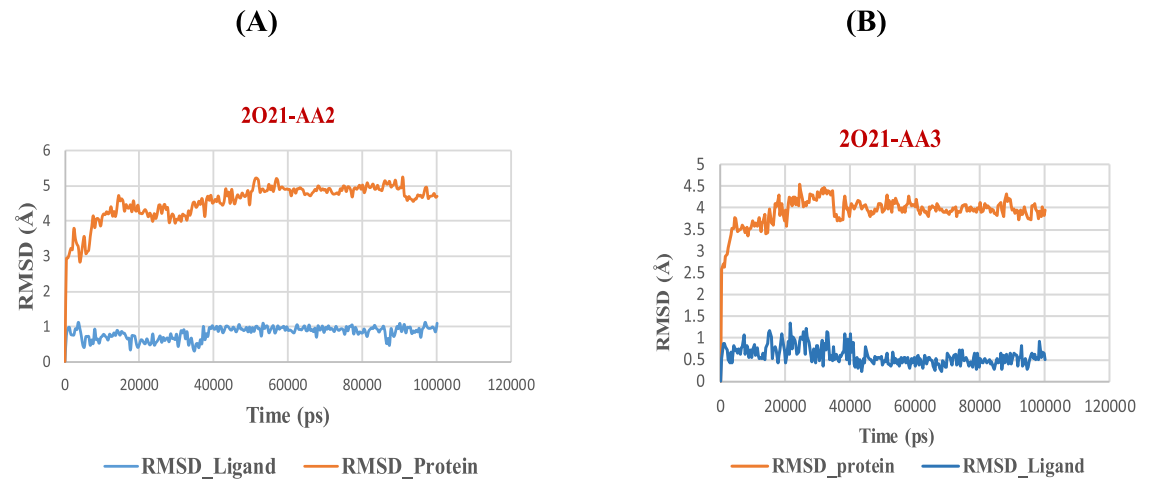

Figure 3. RMSD plots for the complexes: (A) 2O21-AA2 and (B) 2O21-AA3

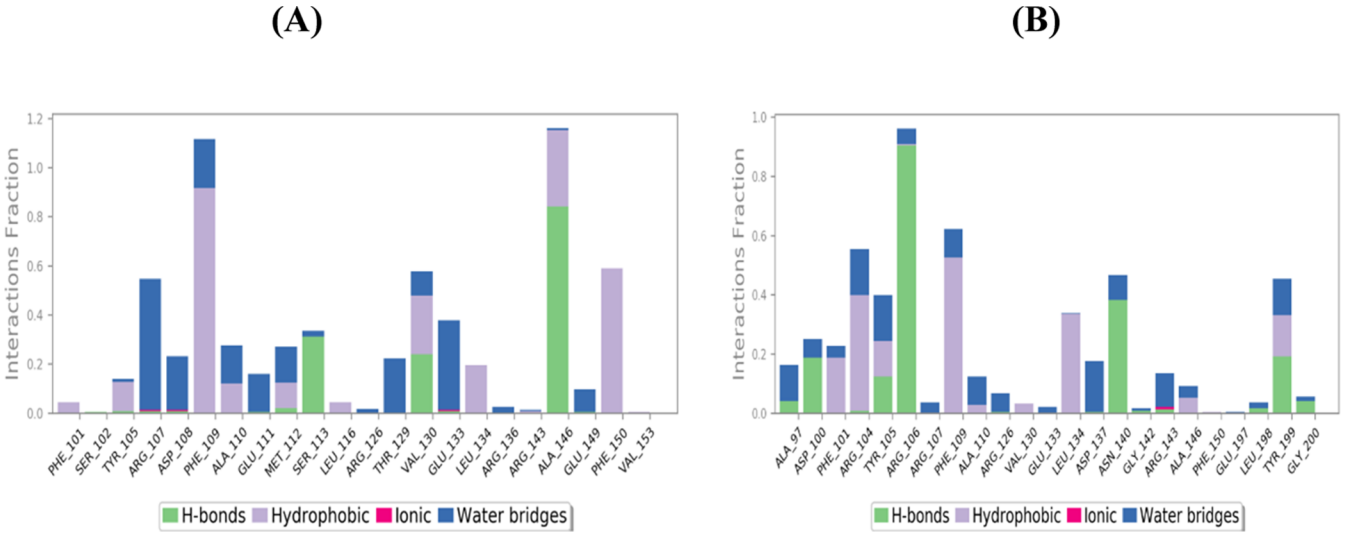

Figure 4. P-L interaction histograms of the complexes: (A) 2O21-AA2 and (B) 2O21-AA3.

2.3.2. Molecular Dynamics Simulation of AA2 and AA3. Complementing our docking studies, we conducted molecular dynamics simulations (MDS) using the Schrödinger−Desmond program to gain insights into the dynamic behavior of protein−ligand complexes. These simulations, spanning 100 ns under the OPLS-2005 force field, allowed us to assess the stability and conformational flexibility of the complexes over time. Analysis of root-mean-square deviation (RMSD) plots revealed consistent stability of the protein (2O21) and the protein−ligand complexes (2O21-AA2 and 2O21-AA3) throughout the simulation trajectories (Figure 3A,B). The RMSD values for the ligands remained below 1 Å, indicating their stable positioning within the binding pockets of the receptor proteins. Despite initial fluctuations, the protein structures eventually stabilized, with RMSD values dropping below 5 Å by the end of the trajectories. Furthermore, examination of protein−ligand histograms provided insights into the prevailing interactions stabilizing the complexes, with hydrogen bonding and hydrophobic interactions emerging as dominant forces governing ligand binding within the protein pockets (Figure 4A,B). Overall, our molecular dynamics simulations provided robust evidence supporting the stability and favorable binding interactions of AA2 and AA3 with their respective target proteins, highlighting their potential as promising anticancer agents.

2.4. Effect of AA2 and AA3 in Inhibiting the Clonogenic Potential of OSCC Cells. Subsequently, we conducted colony formation assay, also known as clonogenic assay, to examine the effects of AA2 and AA3 on the colony-forming potential of SAS cells. Compared with the control group, treatment with both AA2 and AA3 resulted in a marked reduction in colony formation, exhibiting a dose-dependent response. Upon treatment with AA2, SAS cells displayed a significant inhibition of colony formation, with over 50% reduction at a concentration of 2.5 μM. Moreover, the inhibitory effects escalated with increasing concentrations, surpassing 90% inhibition at 5 and 10 μM. Similarly, AA3 treatment also attenuated the clonogenic potential of SAS cells, albeit not exceeding the efficacy of AA2. Nevertheless, at a concentration of 10 μM, AA3 exhibited more than 80% reduction. These findings highlight the significant anticlonogenic activities of AA2 and AA3 in SAS cells (Figure 5A−D). The observed concentration-dependent inhibition of colony formation further substantiates the potential therapeutic efficacy of these compounds in combating OSCC.

https://doi.org/10.1021/acsomega.3c08376
ACS Omega 2024, 9, 24252−24267

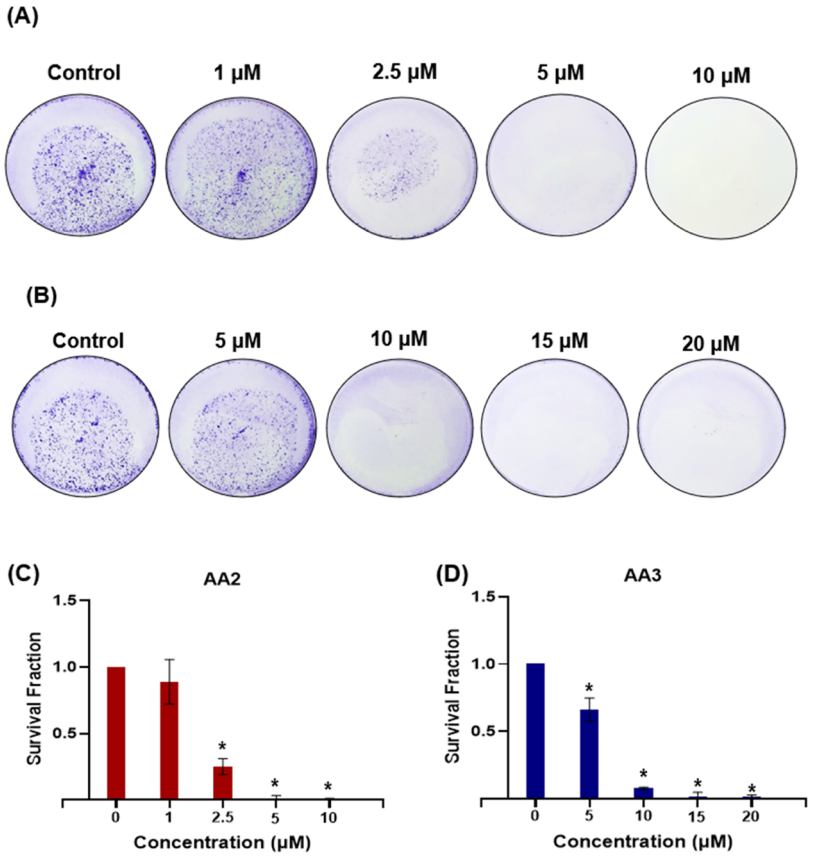

Figure 5. AA2 and AA3 inhibited the clonogenic potential of OSCC cells. SAS cells were treated with different concentrations of (A) AA2 (0, 1, 2.5, 5, and 10 μM) and (B) AA3 (0, 5, 10, 15, 20 μM) for 24 h, and the cells were incubated for 10 days for observing the changes in the colony-forming potential. Survival fraction vs concentration of AA2 (C) and AA3 (D) is plotted. The number of colonies was quantified using ImageJ software and plotted using GraphPad Prism 9.0. Data are presented as mean ± SD, *$p < 0.05$ vs control.

2.5. Effect of AA2 and AA3 in Inducing Cell-Cycle Arrest in OSCC Cells. As AA2 and AA3 inhibited cell proliferation and clonogenic potential, we further evaluated their effects on cell-cycle progression in SAS cells using propidium iodide (PI)-RNase-based flow cytometric analysis. PI is a fluorescent dye that binds to nucleic acids, emitting red fluorescence upon intercalation. This property is utilized in flow cytometry to assess cell viability.[58] We observed that after treatment with AA2 and AA3, the percentage of the cell population in the S-phase increased and that in the G1 and G2 phases decreased significantly in a concentration-dependent manner, indicating the arrest of these cells in the S-phase (Figure 6A−D).

2.6. Effect of AA2 and AA3 in Inducing Cytotoxicity in OSCC Cells. The enduring trait of cellular immortality is one of the widely recognized hallmarks of cancer cells.[59] Therefore, we examined the potential of AA2 and AA3 in inducing cell death in SAS cells by using PI-based flow cytometric analysis. Our results revealed a significant impact of both AA2 and AA3 on the induction of cell death in SAS cells, displaying a concentration-dependent response. We observed that treatment with AA2 at a concentration of 10 μM led to a remarkable cell death of more than 80%. In contrast, AA3, at a concentration of 20 μM, induced approximately 8% cell death (Figure 7A−D). These results attenuate the potent cytotoxic effects of AA2 and AA3 on SAS cells, supporting their potential as agents targeting cancer cell survival mechanisms.

2.7. Effect of AA2 and AA3 in Inducing Apoptosis in OSCC Cells. As AA2 and AA3 were shown to induce cell death, we next examined the apoptosis-inducing ability of these compounds in SAS cells. Annexin V binding and PI uptake assays are widely employed techniques for quantifying apoptosis and necrosis in cellular studies.[60,61] The lipid composition of healthy cells exhibits an asymmetrical distribution in the outer and inner regions of the plasma membrane. Phosphatidylserine (PS), a lipid predominantly situated on the inner region, translocates to the outer region during the initiation of apoptosis.[62] Annexin V, a calcium-binding protein with a molecular weight of 36 kDa, exhibits high affinity for PS.[62] Utilizing the binding specificity of Annexin V for PS, fluorescence-labeled Annexin V serves as a valuable tool for differentiating the cells undergoing apoptosis from those undergoing necrosis. In our investigation, we explored the potential of AA2 and AA3 in inducing apoptosis by employing Annexin V staining, followed by flow cytometric analysis. Comparative analysis with the control group revealed that the treatment of varying concentrations of AA2 on SAS cells led to a dose-dependent escalation of the percentage of apoptotic cells. Specifically, treatment with 2.5 μM AA2 resulted in 8% apoptosis, which increased to 18% at 5 μM and further elevated to 22% at 10 μM. Similarly, AA3 treatment exhibited a parallel trend, with the percentage of apoptotic cells rising from 8% at 5 μM to 18% at 10 μM, 26% at 15 μM, and reaching 30% at 20 μM, respectively (Figure 8A−D). This concentration-dependent increase in apoptosis indicates the significant inhibitory effects

https://doi.org/10.1021/acsomega.3c08376
ACS Omega 2024, 9, 24252−24267

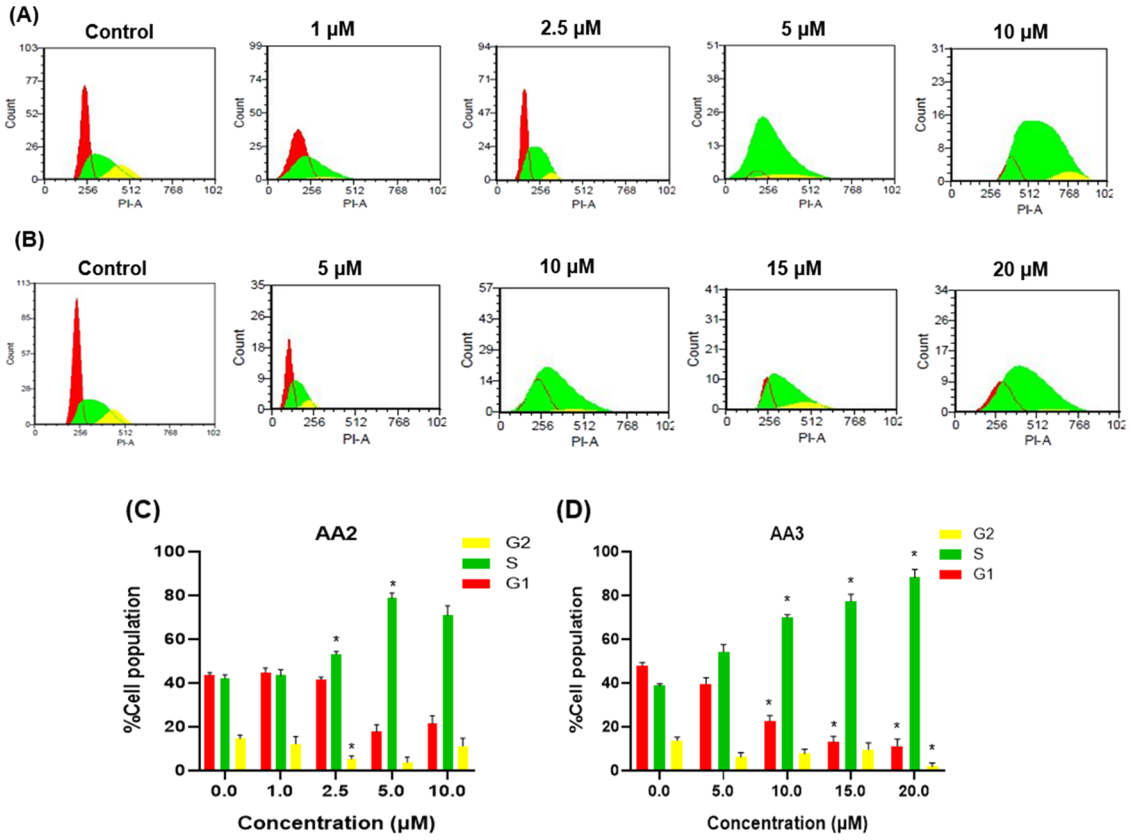

Figure 6. AA2 and AA3 induced cell-cycle arrest in OSCC cells. SAS cells were treated with different concentrations of (A) AA2 (0, 1, 2.5, 5, and 10 μM) and (B) AA3 (0, 5, 10, 15, 20 μM) for 24 h followed by PI-RNase staining and flow cytometric analysis. %cell population vs concentration of AA2 (C) and AA3 (D) is plotted. Percentages of each cell-cycle phase were obtained using FCS Express software. %cell population in each phase was plotted using GraphPad Prism 9.0. Data are presented as mean ± SD, *$p < 0.05$ vs control.

of both AA2 and AA3 on SAS cell survival, suggesting their potential for further investigation as candidates for the development of targeted cancer therapies.

2.8. Effect of AA2 and AA3 on the Migration of OSCC Cells. Next, we investigated the potential of AA2 and AA3 in inhibiting metastasis as they are the primary contributors to cancer-associated mortalities.[63] The effect of AA2 and AA3 in regulating the migration of SAS cells was evaluated by wound-healing assay. In the control cells, wound closure of over 90% was observed within 24 h. In contrast, cells treated with AA2 and AA3 exhibited a markedly diminished migration rate. At the end of 24 h, cells treated with 1 μM AA2 retained approximately 25% of the initial gap, with a concentration-dependent decrease in wound closure observed at higher doses: 40% for 2.5 μM, over 60% for 5 μM, and over 75% for 10 μM-treated cells. Similarly, cells treated with 5 μM AA3 retained over 45% of the gap area, with a progressive increase in wound area persisting at higher concentrations: over 60% for 10 μM, over 65% for 15 μM, and 90% for 20 μM-treated cells. These findings highlighted the substantial potential of both AA2 and AA3 in inhibiting the migration of OSCC cells *in vitro*, as depicted in Figure 9A–D. The observed concentration-dependent effects on wound closure highlight the antimetastatic efficacy of these candidates, positioning them as promising candidates for further exploration in combating cancer metastasis.

2.9. Effect of AA2 and AA3 in Modulating Critical Proteins Responsible for the Development and Progression of OSCC. Studies over the years have reported that multiple proteins including Bcl-2, caspases, COX-2, matrix metalloproteinases (MMPs), survivin, and vascular endothelial growth factor (VEGF) and cell signaling pathways such as Akt/mTOR and signal transducer and activator of transcription 3 (STAT-3) are pivotal in governing various hallmarks of cancer, such as evasion of apoptosis, cell survival, proliferation, invasion, angiogenesis, and migration.[64,65] Abnormal expression of these proteins has been associated with the development and progression of various cancers, including OSCC.[2,66,67]

Bcl-2 is an antiapoptotic protein, and it was found to be overexpressed in OSCC. It was also reported that a diminished level of this protein was associated with a higher survival rate of OSCC patients, and thus, it could be considered a predictor of tumor behavior.[68] Caspases are proapoptotic proteins that can be grouped as either initiator caspases such as caspase-9, which are involved in the initiation of apoptosis, or effector caspases like caspase-3, which causes the degradation of cellular components during apoptosis.[69] Cytochrome c is released from mitochondria, initiating the activation of apaf-1 (apoptosome), which cleaves procaspase-9 into its active dimeric form, caspase-9. Subsequently, activated caspase-9 cleaves caspase-3, which initiates the caspase cascade, resulting in apoptosis.[69,70] Downregulation of caspase-3 and caspase-9 has been reported in various cancers including OSCC.[69,71] Another protein involved in regulating apoptosis in cancer cells is survivin, which functions by inhibiting caspase activation.[72] In OSCC, survivin is consistently expressed across all grades but is notably downregulated in normal oral tissue samples.[73] Overexpression of survivin in HNSCC cells imparts resistance to conventional drugs.[74]

https://doi.org/10.1021/acsomega.3c08376
ACS Omega 2024, 9, 24252−24267

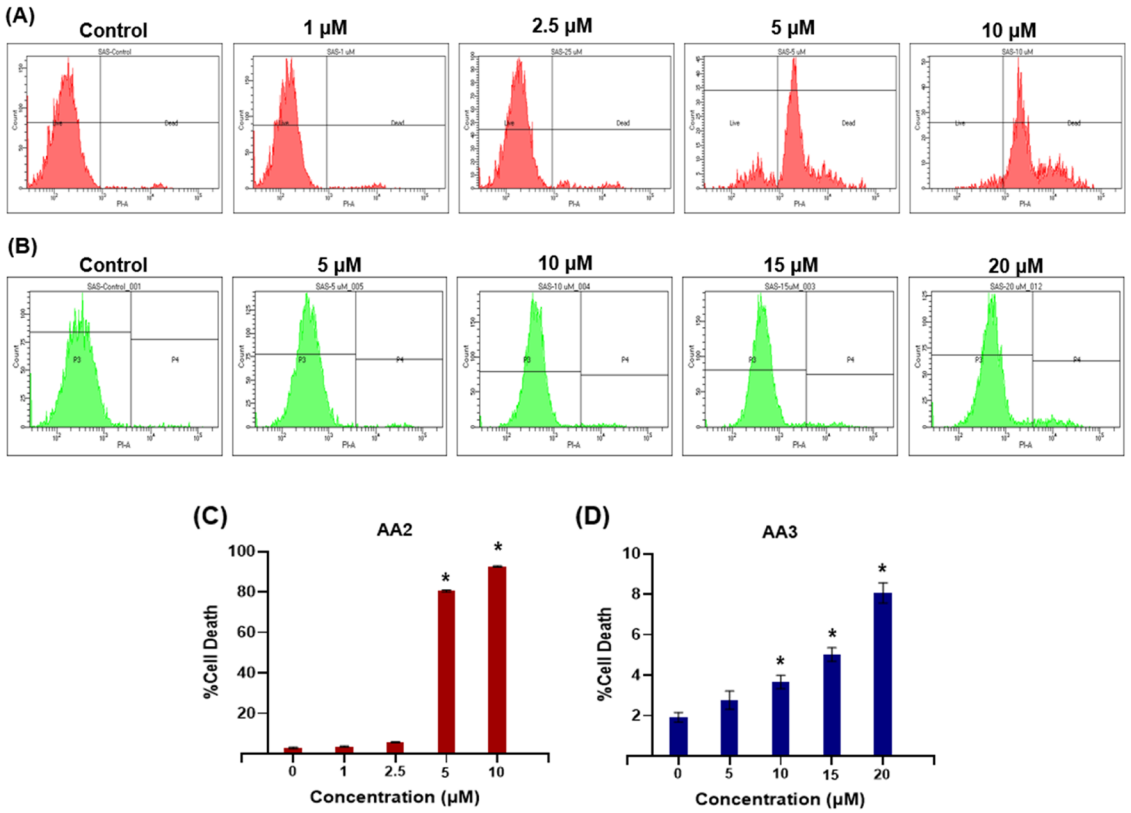

Figure 7. AA2 and AA3 induced cytotoxicity in OSCC cells. SAS cells were treated with different concentrations of (A) AA2 (0, 1, 2.5, 5, and 10 μM) and (B) AA3 (0, 5, 10, 15, 20 μM) for 48 h followed by PI staining and flow cytometric analysis, and %cell death vs concentration of AA2 (C) and AA3 (D) is plotted. %cell death was calculated using BD FACSDiva software and was plotted using GraphPad Prism 9.0. Data are presented as mean ± SD, $^*p < 0.05$ vs control.

COX-2 regulates the initial stage of prostanoid synthesis and is frequently associated with cancer cell survival, proliferation, invasion, angiogenesis, and migration.[75] The elevated expression of COX-2 in dysplastic epithelia and its overexpression in OSCC signify the pivotal role of this enzyme in both the initial phases of oral carcinogenesis and the subsequent events associated with tumor progression.[76] Another protein, VEGF, is pivotal in OSCC progression, fostering invasion and metastasis by inducing morphological changes in blood and lymphatic vessels.[77] VEGF expression is associated with enhanced intratumoral microvessel density, serving as an independent prognostic marker for the overall survival in OSCC patients.[78] MMP-9 emerges as a potential predictive biomarker for the advancement of oral cancer.[79] This proteinase plays a pivotal role in cytoskeletal degradation, which is a critical phase in cancer progression. MMP-9 was reported as a prognostic indicator and suggested that elevated expressions of MMP-9 were notably associated with unfavorable prognosis in oral cancer.[80]

Akt or protein kinase B (PKB) is associated with signal transduction pathways activated by growth factors or insulin, influencing various cellular functions, including cell proliferation, growth, invasion, angiogenesis, and apoptosis.[81] Dysregulation of Akt signaling is associated with poor prognosis in OSCC. Pontes et al. elucidated that the phosphorylation of Akt (p-Akt) constitutes a pivotal event in the progression of potentially malignant lesions, such as oral leukoplakia, toward malignancy.[82] mTOR functions as a conduit for cellular communication regarding synthesis or catabolism, thereby influencing the metabolic processes of proteins, lipids, and nucleotides within cells, ultimately facilitating the provision of necessary resources for cancer growth. Examination of tissue sections from OSCC patients unveiled elevated levels of phosphorylated mTOR (p-mTOR).[83,84] Ribosomal Protein S6 (RPS6) functions as a constituent of the ribosome, the cellular apparatus responsible for the translation of genetic information into proteins. Notably, RPS6 operates under the regulatory influence of the mTOR pathway. It was reported that the activation of RPS6 constitutes an early event in the tumorigenesis process and thus can be considered as a biomarker for the early detection of OSCC.[85]

STAT-3 activation in OSCC leads to cancer cell survival, proliferation, invasion, epithelial-to-mesenchymal transition (EMT), metastasis, immunosuppression, chemoresistance, and poor prognosis.[67] Recent studies have demonstrated the overexpression and constitutive activation of STAT-3 in OSCC, elucidating its pivotal role in driving OSCC aggressiveness. It was also reported that therapeutic strategies targeting STAT-3 led to a reduction in the growth of OSCC cells *in vitro*.[86,87]

Thus, we aimed to evaluate the effects of AA2 and AA3 on the expression of the critical players such as Bcl-2, caspases, COX-2, MMP-9, survivin, VEGF, and cell signaling pathways such as Akt/mTOR and STAT-3 in OSCC. Interestingly, treatment with AA2 and AA3 initiated a cascade of events in the mitochondrial apoptosis machinery. This was evidenced by the activation of caspase-3 and caspase-9 in a dose-dependent manner. Additionally, downregulation of Bcl-2 further substantiated the proapoptotic impact of these compounds. Notably, AA2 and AA3 led to a compelling inhibition of

https://doi.org/10.1021/acsomega.3c08376
ACS Omega 2024, 9, 24252−24267

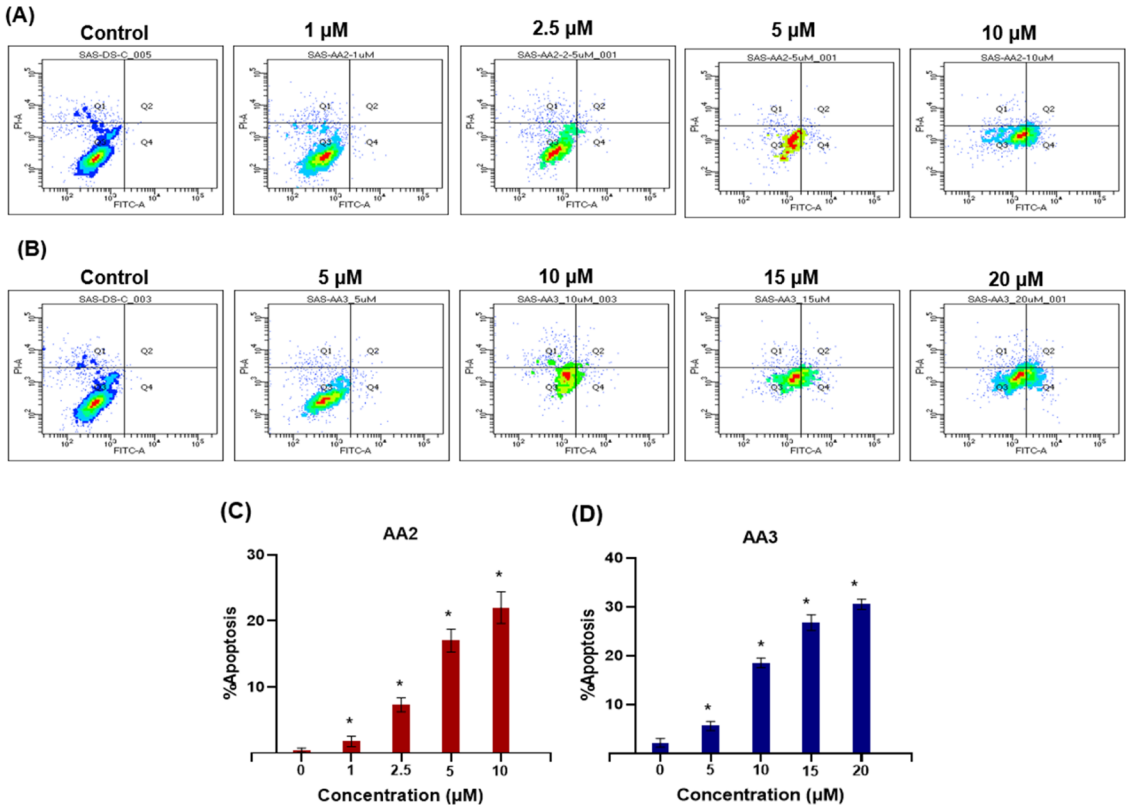

Figure 8. AA2 and AA3 induced apoptosis in OSCC cells. SAS cells were treated with different concentrations of (A) AA2 (0, 1, 2.5, 5, and 10 μM) and (B) AA3 (0, 5, 10, 15, 20 μM) for 48 h followed by Annexin V staining and flow cytometric analysis, and %apoptosis vs concentration of AA2 (C) and AA3 (D) is plotted. %apoptosis was analyzed using BD FACSDiva software, computed from the quadrants Q2+Q4, and plotted using GraphPad Prism 9.0. Data are presented as mean ± SD, $^*p < 0.05$ vs control.

survivin, COX-2, MMP-9, and VEGF-A, suggesting a reduced survival, proliferation, invasion, angiogenesis, and migration of SAS cells. The simultaneous inhibition of the Akt/mTOR and STAT-3 signaling pathways provided compelling evidence supporting the anticancer effects exerted by these compounds (Figures 10 and 11). Taken together, our results revealed that AA2 and AA3 modulated the expression of several critical proteins involved in the development and progression of OSCC (Figure 12).

Accumulating shreds of evidence have shown the anticancer potential of AA2 on different cancers including breast, colon, lung, ovarian, and skin cancers. Notably, most of the studies focus on the potential of this compound in inducing apoptosis via inhibiting the Bcl-2 family of proteins, activating the caspases and ROS production.[39,40,43,44,46,88] This is the first study that demonstrated the ability of AA2 to inhibit the Akt/mTOR and STAT-3 signaling pathways, which are critical and widely associated with the development and progression of OSCC.[2,67] Thus, these findings offer a glimpse into the exact mechanism of action of AA2 and AA3, which can potentially aid in the development of novel therapeutic strategies for combating OSCC.

3. CONCLUSIONS

In summary, this investigation delineates the isolation of two bioactive compounds, namely, artonin E (AA2), a prenylflavone, and artobiloxanthone (AA3), a pyranoxanthone, from the bark of *A. altilis* (Parkinson) Fosberg. These compounds exhibited promising cytotoxicity against the OSCC cell line SAS and were identified through *in vitro* screening assays and *in silico* molecular docking analyses. Subsequent in-depth investigations, encompassing *in vitro* experiments, revealed their distinctive efficacy in inhibiting the proliferation of OSCC cells.

In addition, the mechanistic role of AA2 and AA3 was elucidated, shedding light on their impact on critical proteins implicated in the progression of OSCC. A decrease in the expression of the antiapoptotic protein Bcl-2 and the activation of caspase-3 and caspase-9 cascades were observed, signifying the induction of apoptosis through the mitochondria-mediated pathway. Furthermore, these compounds were found to modulate the Akt/mTOR and STAT-3 signaling pathways in SAS cells. The findings of this study lay a solid foundation for the future exploration of AA2 and AA3 as promising anticancer agents. Thorough and exhaustive investigations will contribute to the development of innovative therapeutic options for OSCC.

4. METHODS

4.1. General Experimental Procedure. The ^{1}H (500 MHz) and ^{13}C (125 MHz) NMR spectra were recorded on a Bruker ASCENDTM-500 MHz NMR spectrometer. Chemical shifts are expressed in δ (ppm) parts using tetramethylsilane (TMS) as an internal standard with solvent deuterated chloroform ($CDCl_3$) having residual peaks at δ_H 7.26 ppm and δ_C 77.30 ppm and with deuterated acetone (CD_3COCD_3) having residual peaks at δ_H 2.05 ppm and δ_C 29.70 and 206.70 ppm, respectively. Coupling constants were in Hz with multiplicity as follows: s, singlet; d, doublet; t, triplet; q, quartet; dd, double doublet; and m, multiplet. Mass spectra were recorded with an Agilent QTOFG6545 spectrometer at 50,000 resolutions using the ESI mode. Column chromatography was

https://doi.org/10.1021/acsomega.3c08376
ACS Omega 2024, 9, 24252−24267

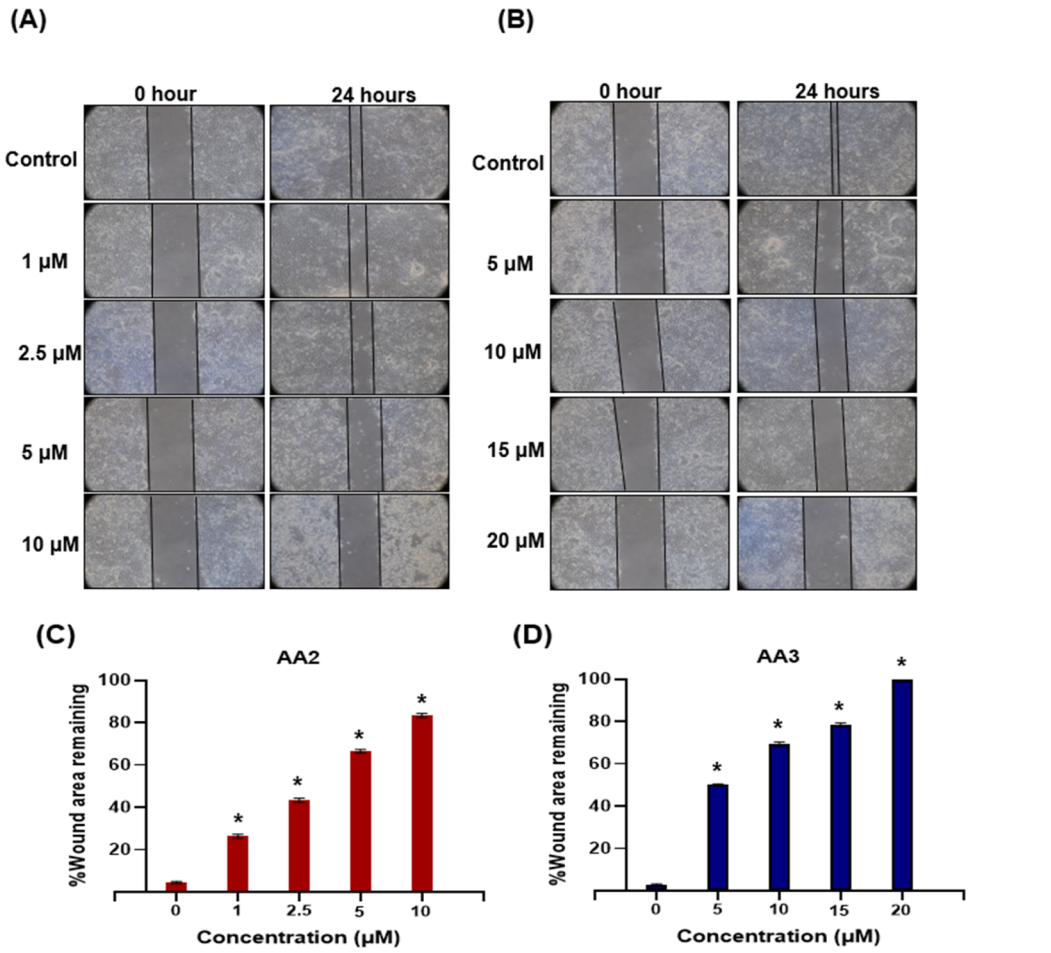

Figure 9. AA2 and AA3 inhibited migration of OSCC cells. SAS cells were treated with different concentrations of (A) AA2 (0, 1, 2.5, 5, and 10 μM) and (B) AA3 (0, 5, 10, 15, 20 μM), followed by the observation of wound areas at 0 and 24 h. %wound area remaining vs concentration of AA2 (C) and AA3 (D) is plotted. Wound areas were calculated with the help of ImageJ software and plotted using GraphPad Prism 9.0. Data are presented as mean ± SD, *p < 0.05 vs control.

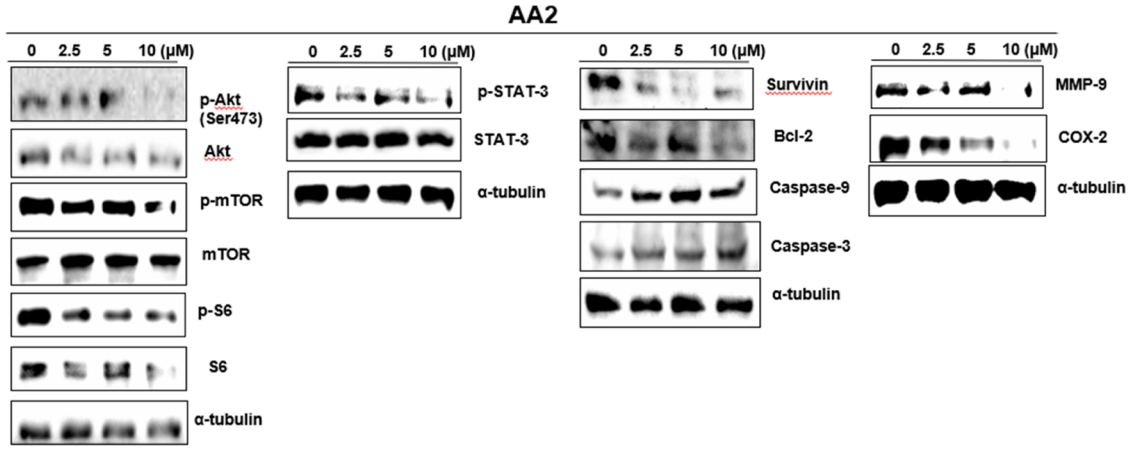

Figure 10. Effect of AA2 on various proteins involved in OSCC. SAS cells were treated with 0, 2.5, 5, and 10 μM concentrations of AA2 for 24 h followed by Western blot analysis. Blots were visualized and analyzed using Image Lab software. α-tubulin was used as the housekeeping control.

performed by using 100−200 and 230−400 mesh silica (Merck, Darmstadt, Germany), and thin-layer chromatography (TLC) was performed by Merck precoated silica gel F_{254} plates. Spots were detected on TLC under UV light and by charring the TLC plate after spraying with p-anisaldehyde-sulfuric acid solution. Reagents and solvents used for column chromatography were purchased from Merck Pvt. Ltd.

4.2. Plant Material. The stem bark of *A. altilis* was collected from Calicut, Kerala, India. The plant material was identified by taxonomists of the Jawaharlal Nehru Botanical Garden of India (JNTBGRI), Palode, Thiruvananthapuram, Kerala.

https://doi.org/10.1021/acsomega.3c08376
ACS Omega 2024, 9, 24252−24267

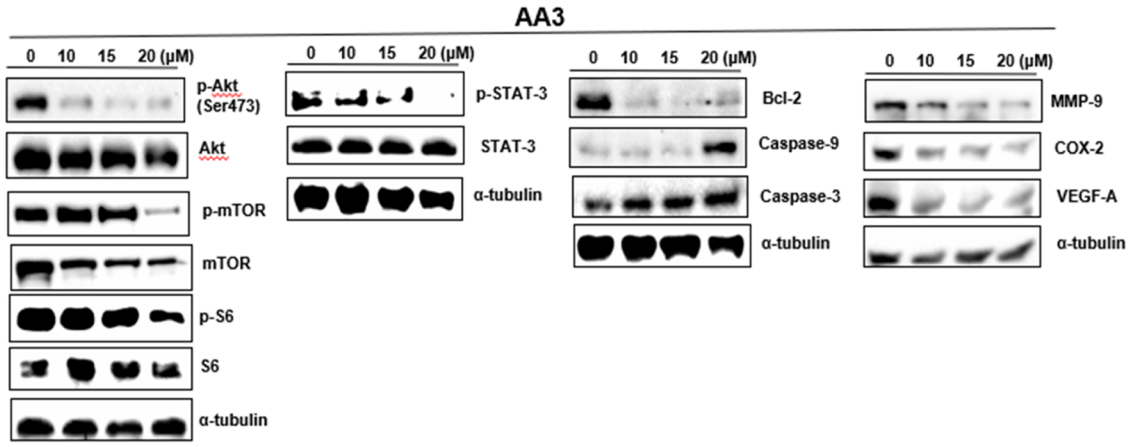

Figure 11. Effect of AA3 on various proteins involved in OSCC. SAS cells were treated with 0, 10, 15, and 20 μM concentrations of AA3 for 24 h followed by Western blot analysis. Blots were visualized and analyzed using Image Lab software. α-tubulin was used as the housekeeping control.

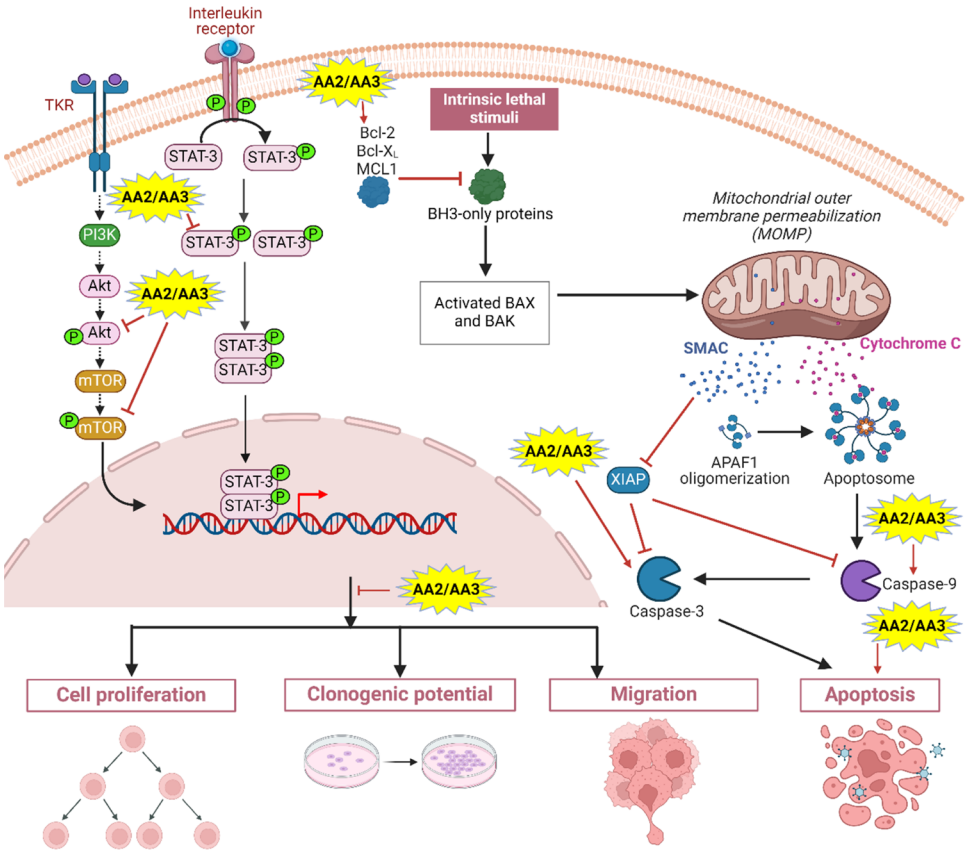

Figure 12. Pathway deciphering the mechanism of action of AA2 and AA3 in OSCC cells. This figure was created with BioRender.com.

4.3. Extraction and Isolation of Phytochemicals. The pulverized material (900 g) was subjected to sequential extraction with hexane, acetone, and ethanol at room temperature for 3 days. The corresponding crude extracts were concentrated using a Heidolph rotary evaporator at a temperature of 50 °C, affording hexane (5 g, 0.5%), acetone (30 g, 3.33%), and ethanol (15 g, 1.66%). The bioactive candidates AA2 and AA3 were isolated and purified from the acetone extracts using conventional silica gel column chromatography using 40 and 30% EtOAc-hexane as the mobile phases together with three flavonoids. The structure of the molecules was confirmed by ^{1}H NMR, ^{13}C NMR, and finally with ESI-HRMS analysis.

4.4. Computational Screening and Molecular Dynamics Simulation. *4.4.1. Computational Screening and Molecular Dynamics Simulation.* The minimization of the proteins and the ligands, the receptor grid generation, and molecular docking were done with Autodock Vina.[89] All of the analyses and visualizations were done using Chimera 1.13 and Maestro13.5.[90] The crystal structures of the proteins were retrieved from the RCSB protein databank.[91] All of these proteins were refined by the addition of hydrogens/missing side chains, assignment of charges, and energy minimization. Grids were then generated encompassing the entire protein structure, facilitating a comprehensive exploration of potential binding sites. To probe the binding interactions, various conformers of

https://doi.org/10.1021/acsomega.3c08376
ACS Omega 2024, 9, 24252−24267

the ligands were selected, allowing for an examination of their binding preferences across different sites. The selection of the optimal conformer was based on its ability to exhibit the highest affinity to a specific protein site, determined through a maximum dock score and the minimum RMSD. Ligand−receptor binding affinities were subsequently ranked based on their dock scores, providing valuable insights into the strength of their interactions.

In order to evaluate the stability and dynamic behavior of the resulting protein−ligand complexes, molecular dynamics simulations were conducted over a duration of 100 ns using the Desmond module of the Schrödinger suite (Desmond Molecular Dynamics System, D. E. Shaw Research, New York, NY, 2021; Maestro-Desmond Interoperability Tools, Schrödinger, New York, NY, 2021). These simulations employed the OPLS-2005 force field, which is known for its accuracy in representing molecular interactions and dynamics. The Desmond Molecular Dynamics System in conjunction with the Maestro-Desmond Interoperability Tools from Schrödinger facilitated the seamless integration and analysis of simulation data, providing crucial insights into the stability and behavior of the protein−ligand complexes.

4.5. Cell Culture. The oral cancer cell line SAS and the normal cell line HaCaT were obtained from RGCB (Rajiv Gandhi Centre for Biotechnology), Trivandrum, and NCCS, Pune, respectively, while the esophageal cancer cell line T.Tn was gifted by Dr. Anirban Bandyopadhyay from the National Institute for Materials Science (NIMS), Japan. The cells were maintained in Dulbecco's minimum essential medium (DMEM; Gibco; Life Technologies, NY) with 10% fetal bovine serum (FBS; Gibco, NY) and 1% Pen-Strep (Invitrogen, CA). The cells were cultured and maintained at 37 °C, 5% CO_2, and 95% humidity unless otherwise stated.

4.6. Cell Proliferation MTT Assay. MTT assay was used to investigate the cytotoxic effect of AA2 and AA3 on SAS, T.Tn, and HaCaT cells and the effect of 5-FU (TCI Pvt. Ltd., India) on SAS cells. Approximately 2×10^3 cells were seeded per well in 96-well plates and incubated for 24 h at 37 °C in a CO_2 incubator. Cells were then treated with AA2 (0,1, 2.5, 5, 10 μM) or AA3 (0, 5, 10, 15, 20 μM) as indicated and incubated for 72 h. 10 μL of 5 mg/mL MTT (Sigma-Aldrich, Missouri) was added to each well and incubated for 2 h. The culture medium was discarded, and 100 μL of DMSO (Merck, Darmstadt, Germany) was added to all of the wells. The absorbance was then measured at 570 nm in a multimode microplate reader (Spectra Max iD3, Molecular Devices). Percentage proliferation (%P) was calculated using the following formula. %P was taken as 100% in the control group.

$$\%P = (\text{absorbance of treated cells}/\text{absorbance of control cells}) \times 100$$

For determining the IC_{50} value, a dose−response curve was constructed with the drug concentration on the X-axis and the corresponding percentage of proliferation on the Y-axis. A straight line was drawn on the graph, starting at the point where Y = 50% (representing 50% inhibition). The line is extended until it intersects with the X-axis. The point where the line intersects the X-axis is taken as the IC_{50} value.

Selectivity index (SI) values for AA2, AA3, and 5-FU were calculated using the following formula:

$$SI = IC_{50}\text{for non-cancerous cell line}/IC_{50}\text{for cancerous cell line}$$

4.7. Colony Formation Assay. Colony formation assay was used to evaluate the effect of AA2 and AA3 on the clonogenic potential of OSCC cells. Briefly, SAS cells were seeded at a density of 2×10^3 cells per well in a 6-well plate and incubated for 24 h at 37 °C in a CO_2 incubator. The following day, AA2 (0, 1, 2.5, 5, 10 μM) or AA3 (0, 5, 10, 15, 20 μM) was added to each well and incubated for 24 h. The medium was then removed and replaced with fresh medium, in which, the cells were cultured for 10 days. The cells were thoroughly washed with 1× PBS thrice and then fixed with 70% ethanol for 4 h at −20 °C. Ethanol was removed, and cells were washed with 1× PBS and stained with 0.01% (w/v) crystal violet (SRL Pvt. Ltd., Mumbai, India). Plates were washed gently to remove the excess stain using 1× PBS. The images of each well were captured using a Nikon digital camera D5100 (Japan). Plating efficiency (PE) and survival fraction (SF) were calculated by using the formula

$$PE = (\text{number of colonies counted}/\text{number of cells plated}) \times 100$$

$$SF = PE\text{ of treated sample}/PE\text{ of control sample}$$

4.8. PI-RNase-Based Cell-Cycle Analysis. PI-RNase-based cell-cycle analysis was performed to evaluate the effect of AA2 and AA3 in inducing cell-cycle arrest in SAS cells. SAS cells were seeded at the density of 2×10^5 cells per well in a 6-well plate and incubated for 24 h at 37 °C in a CO_2 incubator. The cells were then treated with AA2 (0, 1, 2.5, 5, 10 μM) or AA3 (0, 5, 10, 15, 20 μM) for 24 h. Subsequently, the cells were trypsinized, collected, washed with 1× PBS, and then fixed with 75% ethanol overnight at −20 °C. Ethanol was removed by washing with 1× PBS and centrifuging at 4000 rpm for 10 min at 4 °C. The cells were stained with PI-RNase solution and incubated for 20 min in the dark, followed by analysis using a flow cytometer (BD FACSCelesta, Becton-Dickinson, New Jersey). The percentage of cells in each phase of the cell cycle was analyzed using FCS express software and plotted using GraphPad Prism 9.0.

4.9. PI-Based Flow Cytometric Analysis. PI-based flow cytometric analysis was performed to evaluate the effect of AA2 and AA3 in inducing SAS cell death. SAS cells were seeded at the density of 2×10^5 cells per well in a 6-well plate and incubated for 24 h at 37 °C in a CO_2 incubator. The cells were treated with AA2 (0, 1, 2.5, 5, 10 μM) or AA3 (0, 5, 10, 15, 20 μM) and incubated for 48 h. The media were collected in the respective labeled polystyrene test tubes (5 mm × 77 mm), and the cells were trypsinized, collected, and centrifuged at 4000 rpm for 10 min at 4 °C. The supernatant was discarded, and the pellet was washed with 1× PBS and centrifuged again at 4000 rpm for 10 min. This step was repeated three times. The pellet was then suspended in 495 μL of 1× PBS followed by the addition of 5 μL of PI (Sigma-Aldrich, Missouri). The cells were then analyzed in a flow cytometer (BD FACSCelesta, Becton-Dickinson, New Jersey). The percentage of dead cells in each condition was plotted using GraphPad Prism 9.0.

4.10. Annexin V-Based Flow Cytometric Analysis. Annexin V-based flow cytometric analysis was performed to evaluate the effect of AA2 and AA3 in inducing apoptosis in SAS cells. SAS cells were seeded at the density of 2×10^5 cells per well in a 6-well plate and incubated for 24 h at 37 °C in a CO_2

https://doi.org/10.1021/acsomega.3c08376
ACS Omega 2024, 9, 24252−24267

incubator. The cells were then treated with AA2 (0, 1, 2.5, 5, 10 μM) or AA3 (0, 5, 10, 15, 20 μM) and incubated for 48 h. The medium was then collected from all of the wells in the respective labeled polystyrene test tubes. The cells were trypsinized and washed thrice with 1× PBS and centrifuged at 4000 rpm for 10 min at 4 °C. Then, the cells were incubated with 2.5 μL of annexin V for 20 min as per the manufacturer's protocol. 2.5 μL of PI was added to the cells and incubated for 10 min. Analysis was performed using a flow cytometer (BD FACSCelesta, Becton-Dickinson, New Jersey). The percentage of cell population undergoing apoptosis in each condition was plotted using GraphPad Prism 9.0.

4.11. Wound-Healing Assay. The wound-healing scratch assay was performed to evaluate the effect of AA2 and AA3 on the migratory potential of SAS cells. SAS cells were seeded at the density of 6×10^5 cells per well in a 6-well plate and incubated until a monolayer is formed. The medium was then replaced with serum-free DMEM medium and incubated for 6 h to inhibit the proliferation of cells. A scratch was then introduced across the monolayer using a 10 μL tip. The cells were washed with 1x PBS and then treated with either AA2 (0, 1, 2.5, 5, 10 μM) or AA3 (0, 5, 10, 15, 20 μM). The cells were then monitored every 12 h until the migration was completed in the control wells. Images were captured at 0 and 24 h using a Nikon digital camera D5100 (Japan) and analyzed using ImageJ software (NIH, USA). The percentage of the wound area remaining was then plotted using GraphPad Prism 9.0.

4.12. Western Blot Analysis. To evaluate the molecular mechanism behind the anticancer effects of AA2 and AA3, Western blot analysis was performed. SAS cells were seeded at the density of 4×10^5 cells per well in a 6-well plate and incubated for 24 h at 37 °C in a CO_2 incubator. The cells were treated with different concentrations of AA2 (0, 2.5, 5, 10 μM) or AA3 (0, 10, 15, 20 μM). Total protein lysates were prepared using a lysis buffer (2 mM EDTA, 20 mM HEPES buffer, 0.1% (v/v) Triton-X100, 250 mM NaCl, and protease inhibitors including 2 μg/mL aprotinin, 1 mM DTT, 2 μg/mL leupeptin hemisulfate, and 1 mM PMSF). The concentration of protein in the lysates was analyzed using a Bradford protein assay (Bio-Rad, California). Equal concentrations of total protein were then loaded onto a 12% sodium dodecyl sulfate (SDS)-polyacrylamide gel, and electrophoresis was performed at a voltage of 90 V. The gel was then electroblotted onto a nitrocellulose membrane and blocked using 5% nonfat milk powder (Amulya, India). The membrane was then incubated with respective primary antibodies overnight at 4 °C, followed by three times wash with 1× TBST for 10 min each at room temperature. The membrane was then incubated for 2 h with a secondary antibody conjugated with horseradish peroxidase. The membrane was again washed three times with 1× TBST to remove unbound residual secondary antibodies. The blots were developed by adding the Clarity Western ECL substrate (Bio-Rad, California) and using a ChemiDoc XRS System (Bio-Rad, California). Housekeeping gene α-tubulin was used as the loading control.

4.13. Statistical Analysis. Student's t test was employed for statistical analysis, and results are represented as mean ± SD. A value of $p < 0.05$ denoted as "*" was considered statistically significant.

■ ASSOCIATED CONTENT

Supporting Information

The Supporting Information is available free of charge at https://pubs.acs.org/doi/10.1021/acsomega.3c08376.

^{1}H and ^{13}C NMR spectra of AA2 and AA3 and their ESI-high-resolution mass spectra; and molecular docking studies of both AA2 and AA3 with 2O21, IJXQ, and IGFW (PDF)

■ AUTHOR INFORMATION

Corresponding Authors

Ajaikumar B. Kunnumakkara − *Cancer Biology Laboratory, Department of Biosciences and Bioengineering, Indian Institute of Technology Guwahati (IITG), Guwahati 781039 Assam, India;* orcid.org/0000-0001-9121-6816; Email: kunnumakkara@iitg.ac.in

Kokkuvayil Vasu Radhakrishnan − *Chemical Sciences and Technology Division, CSIR-National Institute for Interdisciplinary Science and Technology (CSIR-NIIST), Thiruvananthapuram 695019 Kerala, India; Academy of Scientific and Innovative Research (AcSIR), Ghaziabad 201002 Uttar Pradesh, India;* orcid.org/0000-0001-8909-3175; Email: radhu@niist.res.in

Authors

Maniyamma Aswathy − *Chemical Sciences and Technology Division, CSIR-National Institute for Interdisciplinary Science and Technology (CSIR-NIIST), Thiruvananthapuram 695019 Kerala, India; Academy of Scientific and Innovative Research (AcSIR), Ghaziabad 201002 Uttar Pradesh, India*

Dey Parama − *Cancer Biology Laboratory, Department of Biosciences and Bioengineering, Indian Institute of Technology Guwahati (IITG), Guwahati 781039 Assam, India*

Mangala Hegde − *Cancer Biology Laboratory, Department of Biosciences and Bioengineering, Indian Institute of Technology Guwahati (IITG), Guwahati 781039 Assam, India*

Sherin DR − *Kerala University of Digital Sciences, Innovation and Technology (Digital University Kerala), Thiruvananthapuram 695317 Kerala, India*

Ravi S. Lankalapalli − *Chemical Sciences and Technology Division, CSIR-National Institute for Interdisciplinary Science and Technology (CSIR-NIIST), Thiruvananthapuram 695019 Kerala, India; Academy of Scientific and Innovative Research (AcSIR), Ghaziabad 201002 Uttar Pradesh, India*

Complete contact information is available at: https://pubs.acs.org/10.1021/acsomega.3c08376

Author Contributions

$^{\perp}$M.A. and D.P. contributed equally to this work.

Notes

The authors declare no competing financial interest.

■ ACKNOWLEDGMENTS

The authors acknowledge the BT/556/NE/U-Excel/2016 project awarded by the Department of Biotechnology, Govt. of India. M.A. acknowledges Council of Scientific and Industrial Research (CSIR) for the research fellowship. M.H. acknowledges the Science and Engineering Research Board (SERB), Govt. of India, National Post-Doctoral Fellowship (N-PDF) (PDF/2021/004053), for the financial support. Scheme 1, TOC, and Figure 12 were created with BioRender.com.

■ REFERENCES

(1) Gharat, S. A.; Momin, M.; Bhavsar, C. Oral Squamous Cell Carcinoma: Current Treatment Strategies and Nanotechnology-Based

Approaches for Prevention and Therapy. *Crit. Rev. Ther. Drug Carrier Syst.* **2016**, *33* (4), 363−400.
(2) Harsha, C.; Banik, K.; Ang, H. L.; Girisa, S.; Vikkurthi, R.; Parama, D.; Rana, V.; Shabnam, B.; Khatoon, E.; Kumar, A. P.; Kunnumakkara, A. B. Targeting AKT/mTOR in Oral Cancer: Mechanisms and Advances in Clinical Trials. *Int. J. Mol. Sci.* **2020**, *21* (9), 3285.
(3) Sung, H.; Ferlay, J.; Siegel, R. L.; Laversanne, M.; Soerjomataram, I.; Jemal, A.; Bray, F. Global Cancer Statistics 2020: GLOBOCAN Estimates of Incidence and Mortality Worldwide for 36 Cancers in 185 Countries. *CA. Cancer J. Clin.* **2021**, *71* (3), 209−249.
(4) Chaturvedi, P.; Singh, A.; Chien, C. Y.; Warnakulasuriya, S. Tobacco Related Oral Cancer. *BMJ* **2019**, *365*, l2142.
(5) Chen, P. H.; Mahmood, Q.; Mariottini, G. L.; Chiang, T. A.; Lee, K. W. Adverse Health Effects of Betel Quid and the Risk of Oral and Pharyngeal Cancers. *BioMed Res. Int.* **2017**, *2017*, No. 3904098.
(6) Reidy, J. T.; McHugh, E. E.; Stassen, L. F. A Review of the Role of Alcohol in the Pathogenesis of Oral Cancer and the Link between Alcohol-Containing Mouthrinses and Oral Cancer. *J. Iran Dent. Assoc.* **2011**, *57* (4), 200−202.
(7) Cogliano, V. J.; Baan, R.; Straif, K.; Grosse, Y.; Lauby-Secretan, B.; Ghissassi, F.; El; Bouvard, V.; Benbrahim-Tallaa, L.; Guha, N.; Freeman, C.; Galichet, L.; Wild, C. P. Preventable Exposures Associated with Human Cancers. *J. Natl. Cancer Inst.* **2011**, *103* (24), 1827−1839.
(8) da Silva, S. D.; Hier, M.; Mlynarek, A.; Kowalski, L. P.; Alaoui-Jamali, M. A. Recurrent oral cancer: current and emerging therapeutic approaches. *Front. Pharmacol.* **2012**, *3*, 149.
(9) Monisha, J.; Roy, N. K.; Padmavathi, G.; Banik, K.; Bordoloi, D.; Khwairakpam, A. D.; Arfuso, F.; Chinnathambi, A.; Alahmadi, T. A.; Alharbi, S. A.; Sethi, G.; Kumar, A. P.; Kunnumakkara, A. B. NGAL Is Downregulated in Oral Squamous Cell Carcinoma and Leads to Increased Survival, Proliferation, Migration and Chemoresistance. *Cancers* **2018**, *10* (7), 228.
(10) Banik, K.; Khatoon, E.; Harsha, C.; Rana, V.; Parama, D.; Thakur, K. K.; Bishayee, A.; Kunnumakkara, A. B. Wogonin and Its Analogs for the Prevention and Treatment of Cancer: A Systematic Review. *Phyther. Res.* **2022**, *36* (5), 1854−1883.
(11) Khwairakpam, A. D.; Damayenti, Y. D.; Deka, A.; Monisha, J.; Roy, N. K.; Padmavathi, G.; Kunnumakkara, A. B. Acorus Calamus: A Bio-Reserve of Medicinal Values. *J. Basic Clin. Physiol. Pharmacol.* **2018**, *29* (2), 107−122.
(12) Muralimanoharan, S. B.; Kunnumakkara, A. B.; Shylesh, B.; Kulkarni, K. H.; Haiyan, X.; Ming, H.; Aggarwal, B. B.; Rita, G.; Kumar, A. P. Butanol Fraction Containing Berberine or Related Compound from Nexrutine® Inhibits NFκB Signaling and Induces Apoptosis in Prostate Cancer Cells. *Prostate* **2009**, *69* (5), 494−504.
(13) Ahmed, S. A.; Parama, D.; Daimari, E.; Girisa, S.; Banik, K.; Harsha, C.; Dutta, U.; Kunnumakkara, A. B. Rationalizing the Therapeutic Potential of Apigenin against Cancer. *Life Sci.* **2021**, *267*, No. 118814.
(14) Thomas, D.; Govindhan, S.; Baiju, E. C.; Padmavathi, G.; Kunnumakkara, A. B.; Padikkala, J. Cyperus Rotundus L. Prevents Non-Steroidal Anti-Inflammatory Drug-Induced Gastric Mucosal Damage by Inhibiting Oxidative Stress. *J. Basic Clin. Physiol. Pharmacol.* **2015**, *26* (5), 485−490.
(15) Meenu, M. T.; Kaul, G.; Shukla, M.; Radhakrishnan, K. V.; Chopra, S. Cudraflavone C from Artocarpus Hirsutus as a Promising Inhibitor of Pathogenic, Multidrug-Resistant S. Aureus, Persisters, and Biofilms: A New Insight into a Rational Explanation of Traditional Wisdom. *J. Nat. Prod.* **2021**, *84* (10), 2700−2708.
(16) Meenu, M. T.; Kaul, G.; Akhir, A.; Shukla, M.; Radhakrishnan, K. V.; Chopra, S. Developing the Natural Prenylflavone Artocarpin from Artocarpus Hirsutus as a Potential Lead Targeting Pathogenic, Multidrug-Resistant Staphylococcus Aureus, Persisters and Biofilms with No Detectable Resistance. *J. Nat. Prod.* **2022**, *85* (10), 2413−2423.
(17) Damare, R.; Engle, K.; Kumar, G. Targeting Epidermal Growth Factor Receptor and Its Downstream Signaling Pathways by Natural Products: A Mechanistic Insight. *Phyther. Res.* **2024**, *38*, 2406−2447.
(18) Parama, D.; Girisa, S.; Khatoon, E.; Kumar, A.; Alqahtani, M. S.; Abbas, M.; Sethi, G.; Kunnumakkara, A. B. An Overview of the Pharmacological Activities of Scopoletin against Different Chronic Diseases. *Pharmacol. Res.* **2022**, *179*, No. 106202.
(19) Devi Daimary, U.; Girisa, S.; Parama, D.; Verma, E.; Kumar, A.; Kunnumakkara, A. B. Embelin: A Novel XIAP Inhibitor for the Prevention and Treatment of Chronic Diseases. *J. Biochem. Mol. Toxicol.* **2022**, *36* (2), No. e22950.
(20) Girisa, S.; Parama, D.; Harsha, C.; Banik, K.; Kunnumakkara, A. B. Potential of Guggulsterone, a Farnesoid X Receptor Antagonist, in the Prevention and Treatment of Cancer. *Explor. Targeted Anti-Tumor Ther.* **2020**, *1* (5), 313−342.
(21) Parama, D.; Rana, V.; Girisa, S.; Verma, E.; Daimary, U. D.; Thakur, K. K.; Kumar, A.; Kunnumakkara, A. B. The Promising Potential of Piperlongumine as an Emerging Therapeutics for Cancer. *Explor. Targeted Anti-Tumor Ther.* **2021**, *2* (4), 323−354.
(22) Kunnumakkara, A. B.; Nair, A. S.; Kwang, S. A.; Pandey, M. K.; Yi, Z.; Liu, M.; Aggarwal, B. B. Gossypin, a Pentahydroxy Glucosyl Flavone, Inhibits the Transforming Growth Factor Beta-Activated Kinase-1-Mediated NF-KB Activation Pathway, Leading to Potentiation of Apoptosis, Suppression of Invasion, and Abrogation of Osteoclastogenesis. *Blood* **2007**, *109* (12), 5112−5121.
(23) Tariq, A.; Sadia, S.; Pan, K.; Ullah, I.; Mussarat, S.; Sun, F.; Abiodun, O. O.; Batbaatar, A.; Li, Z.; Song, D.; Xiong, Q.; Ullah, R.; Khan, S.; Basnet, B. B.; Kumar, B.; Islam, R.; Adnan, M. A Systematic Review on Ethnomedicines of Anti-Cancer Plants. *Phyther. Res.* **2017**, *31* (2), 202−264.
(24) Khatoon, E.; Banik, K.; Harsha, C.; Sailo, B. L.; Thakur, K. K.; Khwairakpam, A. D.; Vikkurthi, R.; Devi, T. B.; Gupta, S. C.; Kunnumakkara, A. B. Phytochemicals in Cancer Cell Chemosensitization: Current Knowledge and Future Perspectives. *Semin. Cancer Biol.* **2022**, *80*, 306−339.
(25) Banik, K.; Ranaware, A. M.; Harsha, C.; Nitesh, T.; Girisa, S.; Deshpande, V.; Fan, L.; Nalawade, S. P.; Sethi, G.; Kunnumakkara, A. B. Piceatannol: A Natural Stilbene for the Prevention and Treatment of Cancer. *Pharmacol. Res.* **2020**, *153*, No. 104635.
(26) Kunnumakkara, A. B.; Anand, P.; Aggarwal, B. B. Curcumin Inhibits Proliferation, Invasion, Angiogenesis and Metastasis of Different Cancers through Interaction with Multiple Cell Signaling Proteins. *Cancer Lett.* **2008**, *269* (2), 199−225.
(27) Sultana, H.; Chetia, A.; Saikia, A.; Khan, N. J. An Updated Review on Extraction, Isolation, and Identification of Bioactive Compounds from Plant Extracts. *Sch. Acad. J. Pharm.* **2023**, *12* (07), 154−171.
(28) Aswathy, M.; Banik, K.; Parama, D.; Sasikumar, P.; Harsha, C.; Joseph, A. G.; Sherin, D. R.; Thanathu, M. K.; Kunnumakkara, A. B.; Vasu, R. K. Exploring the Cytotoxic Effects of the Extracts and Bioactive Triterpenoids from Dillenia Indica against Oral Squamous Cell Carcinoma: A Scientific Interpretation and Validation of Indigenous Knowledge. *ACS Pharmacol. Transl. Sci.* **2021**, *4* (2), 834−847.
(29) Jagtap, U. B.; Bapat, V. A. *Artocarpus*: A Review of Its Traditional Uses, Phytochemistry and Pharmacology. *J. Ethnopharmacol.* **2010**, *129* (2), 142−166.
(30) Nomura, T.; Hano, Y.; Aida, M. Isoprenoid-Substituted Flavonoids from *Artocarpus* Plants (Moraceae). *Heterocycles* **1998**, *47* (2), 1179−1205.
(31) Hakim, E. H.; Achmad, S. A.; Juliawaty, L. D.; Makmur, L.; Syah, Y. M.; Aimi, N.; Kitajima, M.; Takayama, H.; Ghisalberti, E. L. Prenylated Flavonoids and Related Compounds of the Indonesian *Artocarpus* (Moraceae). *J. Nat. Med.* **2006**, *60* (3), 161−184.
(32) Sikarwar, M. S.; Hui, B. J.; Subramaniam, K.; Valeisamy, B. D.; Yean, L. K.; Balaji, K. A Review on *Artocarpus altilis* (Parkinson) Fosberg (Breadfruit). *J. Appl. Pharm. Sci.* **2014**, *4* (8), 91−97.
(33) Zajmi, A.; Mohd Hashim, N.; Noordin, M. I.; Khalifa, S. A. M.; Ramli, F.; Mohd Ali, H.; El-Seedi, H. R. Ultrastructural Study on the Antibacterial Activity of Artonin e versus Streptomycin against *Staphylococcus aureus* Strains. *PLoS One* **2015**, *10* (6), No. e0128157.
(34) Chan, E. W. C. Artonin E: A Short Review of Its Chemistry, Sources, Anti-Cancer Activities and Other Pharmacological Properties. *Trop. J. Nat. Prod. Res.* **2023**, *7* (6), 3051−3058.

https://doi.org/10.1021/acsomega.3c08376
ACS Omega 2024, 9, 24252−24267

(35) Fukai, T.; Satoh, K.; Nomura, T.; Sakagami, H. Antinephritis and Radical Scavenging Activity of Prenylflavonoids. *Fitoterapia* **2003**, *74* (7−8), 720−724.
(36) Chaturvedi, I. Molecular Docking Study to Find Natural Inhibitor Against FAT10 Protein for Curing Hepatic Carcinoma. *J. Sci.* **2015**, *1* (2), 1−43.
(37) Hidayati, A. R.; Widyawaruyanti, A.; Ilmi, H.; Tanjung, M.; Widiandani, T.; Siswandono; Syafruddin, D.; Hafid, A. F. Antimalarial Activity of Flavonoid Compound Isolated from Leaves of *Artocarpus altilis*. *Pharmacogn. J.* **2020**, *12* (4), 835−842.
(38) Suhartati, T.; Yandri; Suwandp, J. F.; Hadi, S. In Vitro and in Vivo Antiplasmodial Activity of Oxyresveratrol and Artonin E Isolated from Two Artocarpus Plants in Indonesia. *Orient. J. Chem.* **2010**, *26* (3), 825−830.
(39) Etti, I. C.; Rasedee, A.; Mohd Hashim, N.; Abdul, A. B.; Kadir, A.; Yeap, S. K.; Waziri, P.; Malami, I.; Lim, K. L.; Etti, C. J. Artonin E Induces p53-Independent G1 Cell Cycle Arrest and Apoptosis through ROS-Mediated Mitochondrial Pathway and Livin Suppression in MCF-7 Cells. *Drug Des. Devel. Ther.* **2017**, *11*, 865−879.
(40) Etti, I. C.; Abdullah, R.; Kadir, A.; Hashim, N. M.; Yeap, S. K.; Imam, M. U.; Ramli, F.; Malami, I.; Lam, K. L.; Etti, U.; Waziri, P.; Rahman, M. The Molecular Mechanism of the Anticancer Effect of Artonin E in MDA-MB 231 Triple Negative Breast Cancer Cells. *PLoS One* **2017**, *12* (8), No. e0182357.
(41) Sophonnithiprasert, T.; Mahabusarakam, W.; Watanapokasin, R. Artonin E Sensitizes TRAIL-Induced Apoptosis by DR5 Upregulation and CFLIP Downregulation in TRAIL-Refractory Colorectal Cancer LoVo Cells. *J. Gastrointest. Oncol.* **2019**, *10* (2), 209−217.
(42) Yangnok, K.; Innajak, S.; Sawasjirakij, R.; Mahabusarakam, W.; Watanapokasin, R. Effects of Artonin E on Cell Growth Inhibition and Apoptosis Induction in Colon Cancer LoVo and HCT116 Cells. *Molecules* **2022**, *27* (7), 2095.
(43) Toume, K.; Habu, T.; Arai, M. A.; Koyano, T.; Kowithayakorn, T.; Ishibashi, M. Prenylated Flavonoids and Resveratrol Derivatives Isolated from Artocarpus Communis with the Ability to Overcome TRAIL Resistance. *J. Nat. Prod.* **2015**, *78* (1), 103−110.
(44) Musthapa, I.; Latip, J.; Takayama, H.; Juliawaty, L. D.; Hakim, E. H.; Syah, Y. M. Prenylated Flavones from Artocarpus Lanceifolius and Their Cytotoxic Properties against P-388 Cells. *Nat. Prod. Commun.* **2009**, *4* (7), 927−930.
(45) Plaibua, K.; Pongrakhananon, V.; Chunhacha, P.; Sritularak, B.; Chanvorachote, P. Effects of Artonin E on Migration and Invasion Capabilities of Human Lung Cancer Cells. *Anticancer Res.* **2013**, *33* (8), 3079−3088. PMID: 23898063
(46) Wongpankam, E.; Chunhacha, P.; Pongrakhananon, V.; Sritularak, B.; Chanvorachote, P. Artonin E Mediates MCL1 Down-Regulation and Sensitizes Lung Cancer Cells to Anoikis. *Anticancer Res.* **2012**, *32* (12), 5343−5351. PMID: 23225436
(47) Rahman, M. A.; Ramli, F.; Karimian, H.; Dehghan, F.; Nordin, N.; Mohd Ali, H.; Mohan, S.; Mohd Hashim, N. Artonin E Induces Apoptosis via Mitochondrial Dysregulation in SKOV-3 Ovarian Cancer Cells. *PLoS One* **2016**, *11* (3), No. e0151466.
(48) Rahman, M. A.; Hashim, N. M. Apoptotic Induction Mechanism of Artonin E in 3D Ovarian Cancer Cell Lines. *Indones. J. Pharm.* **2022**, *33* (1), 147−158.
(49) Tang, W.; Wang, W.; Zhang, Y.; Liu, S.; Liu, Y.; Zheng, D. Tumour Necrosis Factor-Related Apoptosis-Inducing Ligand (TRAIL)-Induced Chemokine Release in Both TRAIL-Resistant and TRAIL-Sensitive Cells via Nuclear Factor Kappa B. *FEBS J.* **2009**, *276* (2), 581−593.
(50) Metabocard for Artobiloxanthone (HMDB0034021) *1* 14.
(51) Parvatikar, P. P.; Madagi, S. B.Molecular Docking Analysis: Interaction Studies of Natural Compounds with Human TG2 Protein. In *Transactions on Engineering Technologies*; Springer, 2021; pp 101−111 DOI: 10.1007/978-981-15-6848-0.
(52) Seo, E. K.; Lee, D.; Young, G. S.; Chai, H. B.; Navarro, H. A.; Kardono, L. B. S.; Rahman, I.; Cordell, G. A.; Farnsworth, N. R.; Pezzuto, J. M.; Kinghorn, A. D.; Wani, M. C.; Wall, M. E. Bioactive Prenylated Flavonoids from the Stem Bark of Artocarpus Kemando. *Arch. Pharm. Res.* **2003**, *26* (2), 124−127.
(53) Indrayanto, G.; Putra, G. S.; Suhud, F. *Validation of In-Vitro Bioassay Methods: Application in Herbal Drug Research*, 1st ed.; Elsevier Inc, 2021; Vol. *46* DOI: 10.1016/bs.podrm.2020.07.005.
(54) Weerapreeyakul, N.; Nonpunya, A.; Barusrux, S.; Thitimetharoch, T.; Sripanidkulchai, B. Evaluation of the Anticancer Potential of Six Herbs against a Hepatoma Cell Line. *Chin. Med.* **2012**, *7* (1), 15.
(55) Harada, K.; Ferdous, T.; Ueyama, Y. Establishment of 5-Fluorouracil-Resistant Oral Squamous Cell Carcinoma Cell Lines with Epithelial to Mesenchymal Transition Changes. *Int. J. Oncol.* **2014**, *44* (4), 1302−1308.
(56) Negarandeh, R.; Salehifar, E.; Saghafi, F.; Jalali, H.; Janbabaei, G.; Abdhaghighi, M. J.; Nosrati, A. Evaluation of Adverse Effects of Chemotherapy Regimens of 5-Fluoropyrimidines Derivatives and Their Association with DPYD Polymorphisms in Colorectal Cancer Patients. *BMC Cancer* **2020**, *20* (1), 560.
(57) Wigmore, P. M.; Mustafa, S.; El-Beltagy, M.; Lyons, L.; Umka, J.; Bennett, G. Effects of 5-FU. *Adv. Exp. Med. Biol.* **2010**, *678*, 157−164.
(58) Crowley, L. C.; Scott, A. P.; Marfell, B. J.; Boughaba, J. A.; Chojnowski, G.; Waterhouse, N. J. Measuring Cell Death by Propidium Iodide Uptake and Flow Cytometry. *Cold Spring Harb. Protoc.* **2016**, *2016* (7), 647−651.
(59) Hanahan, D. Hallmarks of Cancer: New Dimensions. *Cancer Discovery* **2022**, *12* (1), 31−46.
(60) Reutelingsperger, C. P. M.; Van Heerde, W. L. Annexin V, the Regulator of Phosphatidylserine-Catalyzed Inflammation and Coagulation during Apoptosis. *Cell. Mol. Life Sci.* **1997**, *53* (6), 527−532.
(61) Komoriya, A.; Packard, B. Z.; Brown, M. J.; Wu, M. L.; Henkart, P. A. Assessment of Caspase Activities in Intact Apoptotic Thymocytes Using Cell-Permeable Fluorogenic Caspase Substrates. *J. Exp. Med.* **2000**, *191* (11), 1819−1828.
(62) Walker, J. H.; Boustead, C. M.; Koster, J. J.; Bewley, M.; Waller, D. A. Annexin V, a Calcium-Dependent Phospholipid-Binding Protein. *Biochem. Soc. Trans.* **1992**, *20* (4), 828−833.
(63) Fares, J.; Fares, M. Y.; Khachfe, H. H.; Salhab, H. A.; Fares, Y. Molecular Principles of Metastasis: A Hallmark of Cancer Revisited. *Signal Transduction Target. Ther.* **2020**, *5* (1), 28.
(64) Pei, H.; Guo, W.; Peng, Y.; Xiong, H.; Chen, Y. Targeting Key Proteins Involved in Transcriptional Regulation for Cancer Therapy: Current Strategies and Future Prospective. *Med. Res. Rev.* **2022**, *42*, 1607−1660, DOI: 10.1002/med.21886.
(65) Kampen, K. R. Membrane Proteins: The Key Players of a Cancer Cell. *J. Membr. Biol.* **2011**, *242* (2), 69−74.
(66) Girisa, S.; Kumar, A.; Rana, V.; Parama, D.; Daimary, U. D.; Warnakulasuriya, S.; Kumar, A. P.; Kunnumakkara, A. B. From Simple Mouth Cavities to Complex Oral Mucosal Disorders - Curcuminoids as a Promising Therapeutic Approach. *ACS Pharmacol. Transl. Sci.* **2021**, *4* (2), 647−665.
(67) Khatoon, E.; Hegde, M.; Kumar, A.; Daimary, U. D.; Sethi, G.; Bishayee, A.; Kunnumakkara, A. B. The Multifaceted Role of STAT3 Pathway and Its Implication as a Potential Therapeutic Target in Oral Cancer. *Arch. Pharm. Res.* **2022**, *45* (8), 507−534.
(68) Popović, B.; Jekić, B.; Novaković, I.; Luković, L. J.; Tepavčević, Z.; Jurišić, V.; Vukadinović, M.; Milašin, J. Bcl-2 Expression in Oral Squamous Cell Carcinoma. *Ann. N.Y. Acad. Sci.* **2007**, *1095*, 19−25.
(69) Dwivedi, R.; Pandey, R.; Chandra, S.; Mehrotra, D. Apoptosis and Genes Involved in Oral Cancer - a Comprehensive Review. *Oncol. Rev.* **2020**, *14* (2), 472.
(70) Li, P.; Nijhawan, D.; Budihardjo, I.; Srinivasula, S. M.; Ahmad, M.; Alnemri, E. S.; Wang, X. Cytochrome c and DATP-Dependent Formation of Apaf-1/Caspase-9 Complex Initiates an Apoptotic Protease Cascade. *Cell* **1997**, *91* (4), 479−489.
(71) Ding, H.; Han, C.; Zhu, J.; Chen, C. S.; D'Ambrosio, S. M. Celecoxib Derivatives Induce Apoptosis via the Disruption of Mitochondrial Membrane Potential and Activation of Caspase 9. *Int. J. Cancer* **2005**, *113* (5), 803−810.

(72) Kulkarni, D. P.; Shah, V.; Sinha, S.; Patel, J. Immunohistochemical Expression Of Survivin In Different Grades Of Oral Squamous Cell Carcinoma. *IOSR J. Dent. Med. Sci.* **2017**, *16* (7), 75−79.
(73) Ajithkumar, M.; Murali, C. R.; Vani, N. V. Prognostic Implication of Survivin Expression in Oral Squamous Cell Carcinoma-An Immunohistochemical Study. *J. Contemp. Dent. Pract.* **2019**, *20* (5), 577−581.
(74) Khan, Z.; Khan, A. A.; Yadav, H.; Prasad, G. B. K. S.; Bisen, P. S. Survivin, a Molecular Target for Therapeutic Interventions in Squamous Cell Carcinoma. *Cell. Mol. Biol. Lett.* **2017**, *22*, 8.
(75) Liu, B.; Qu, L.; Yan, S. Cyclooxygenase-2 Promotes Tumor Growth and Suppresses Tumor Immunity. *Cancer Cell Int.* **2015**, *15* (1), 106.
(76) Shibata, M.; Kodani, I.; Osaki, M.; Araki, K.; Adachi, H.; Ryoke, K.; Ito, H. Cyclo-Oxygenase-1 and −2 Expression in Human Oral Mucosa, Dysplasias and Squamous Cell Carcinomas and Their Pathological Significance. *Oral Oncol.* **2005**, *41* (3), 304−312.
(77) Abdul-Aziz, M. A.; Amin, A. K.; El-Rouby, D. H.; Shaker, O. G. Lymphangiogenesis in Oral Squamous Cell Carcinoma: Correlation with VEGF-C Expression and Lymph Node Metastasis. *Int. J. Dent.* **2017**, *2017*, No. 7285656.
(78) Niklander, S.; Bordagaray, M. J.; Fernández, A.; Hernández, M. Vascular Endothelial Growth Factor: A Translational View in Oral Non-Communicable Diseases. *Biomolecules* **2021**, *11* (1), 85.
(79) Saini, J.; Bakshi, J.; Panda, N. K.; Sharma, M.; Yadav, A. K.; Kamboj, K.; Goyal, A. K. Serum Concentration of MMP-9 as a Predictive Biomarker for the Progression of Oral Cancer. *J. Maxillofac. Oral Surg.* **2023**, 1−1.
(80) Deng, W.; Peng, W.; Wang, T.; Chen, J.; Zhu, S. Overexpression of MMPs Functions as a Prognostic Biomarker for Oral Cancer Patients: A Systematic Review and Meta-analysis. *Oral Health Prev. Dent.* **2019**, *17* (6), 505−514.
(81) Robbins, H. L.; Hague, A. The PI3K/Akt Pathway in Tumors of Endocrine Tissues. *Front. Endocrinol.* **2016**, *6*, 188.
(82) Pontes, H. A. R.; De Aquino Xavier, F. C.; Da Silva, T. S. P.; Fonseca, F. P.; Paiva, H. B.; Pontes, F. S. C.; Dos Santos Pinto, D. Metallothionein and P-Akt Proteins in Oral Dysplasia and in Oral Squamous Cell Carcinoma: An Immunohistochemical Study. *J. Oral Pathol. Med.* **2009**, *38* (8), 644−650.
(83) Li, S. H.; Chien, C. Y.; Huang, W. T.; Luo, S. D.; Su, Y. Y.; Tien, W. Y.; Lan, Y. C.; Chen, C. H. Prognostic Significance and Function of Mammalian Target of Rapamycin in Tongue Squamous Cell Carcinoma. *Sci. Rep.* **2017**, *7* (1), No. 8178, DOI: 10.1038/s41598-017-08345-8.
(84) Naruse, T.; Yanamoto, S.; Yamada, S.-i.; Rokutanda, S.; Kawakita, A.; Kawasaki, G.; Umeda, M. Anti-Tumor Effect of the Mammalian Target of Rapamycin Inhibitor Everolimus in Oral Squamous Cell Carcinoma. *Pathol. Oncol. Res.* **2015**, *21* (3), 765−773, DOI: 10.1007/s12253-014-9888-1.
(85) Chaisuparat, R.; Rojanawatsirivej, S.; Yodsanga, S. Ribosomal Protein S6 Phosphorylation Is Associated with Epithelial Dysplasia and Squamous Cell Carcinoma of the Oral Cavity. *Pathol. Oncol. Res.* **2013**, *19* (2), 189−193.
(86) Leong, P. L.; Andrews, G. A.; Johnson, D. E.; Dyer, K. F.; Xi, S.; Mai, J. C.; Robbins, P. D.; Gadiparthi, S.; Burke, N. A.; Watkins, S. F.; Grandis, J. R. Targeted Inhibition of Stat3 with a Decoy Oligonucleotide Abrogates Head and Neck Cancer Cell Growth. *Proc. Natl. Acad. Sci. U. S. A.* **2003**, *100* (7), 4138−4143.
(87) Klosek, S. K.; Nakashiro, K.-I.; Hara, S.; Goda, H.; Hamakawa, H. Stat3 as a Molecular Target in RNA Interference-Based Treatment of Oral Squamous Cell Carcinoma. *Oncol. Rep.* **2008**, *20*, 873−878, DOI: 10.3892/or.
(88) Innajak, S.; Tangchirakhaphan, S.; Nilwarangoon, S.; Tanjapatkul, N.; Mahabusarakam, W.; Watanapokasin, R. Anti-Proliferation and Apoptosis Induction in Epidermoid Carcinoma A431 Cells by Artonin E. *J. Med. Assoc. Thailand* **2017**, *100* (10), S54−S60.
(89) Trott, O.; Olson, A. J. AutoDock Vina: Improving the Speed and Accuracy of Docking with a New Scoring Function, Efficient Optimization, and Multithreading. *J. Comput. Chem.* **2010**, *31* (2), 455−461.
(90) Pettersen, E. F.; Goddard, T. D.; Huang, C. C.; Couch, G. S.; Greenblatt, D. M.; Meng, E. C.; Ferrin, T. E. UCSF Chimera - A Visualization System for Exploratory Research and Analysis. *J. Comput. Chem.* **2004**, *25* (13), 1605−1612.
(91) https://www.rcsb.Org/.

https://doi.org/10.1021/acsomega.3c08376
ACS Omega 2024, 9, 24252−24267